INTERNATIONAL JOURNAL FOR NUMERICAL METHODS IN ENGINEERING
Int. J. Numer. Meth. Engng (2010)
Published online in Wiley Online Library (wileyonlinelibrary.com). DOI: 10.1002/nme.3089

Complementary geometric formulations for electrostatics

Ruben Specogna*, †

Dipartimento di Ingegneria Elettrica, Gestionale e Meccanica (DIEGM), Università di Udine, Via delle Scienze 208, I-33100 Udine, Italy

SUMMARY

The simultaneous use of a pair of complementary discrete formulations for electrostatic boundary value problems (BVPs) allows to accurately compute electromagnetic quantities, such as capacitance or electrostatic force with a minimum computational effort. In fact, the two formulations provide the upper and lower bounds for these quantities and their averages result quite close to the exact solution even for extremely coarse meshes. Despite the potential benefit to the many three-dimensional large-scale applications, taking advantage of this feature is not exploited in practice due to theoretical difficulties in the potential design.

The aim of this paper is to fill this gap by rigorously introducing a pair of three-dimensional complementary geometric formulations to solve electrostatic BVPs on domains covered by *conformal polyhedral meshes*. In particular, an original formulation based on a vector potential is introduced by using cohomology theory with integer coefficients. It is shown how the so-called *thick links* are needed, which are representatives of the second cohomology group generators of the dielectric region. Two easy-to-implement graph-theoretic algorithms to automatically find such a basis with optimal computational complexity are described. Some benchmark problems are presented to show how the simultaneous use of both formulations yields to a sensible computational advantage. Therefore, solvers based on complementary formulations should be embedded in the next-generation of electromagnetic Computer-Aided Engineering (CAE) softwares. Copyright © 2010 John Wiley & Sons, Ltd.

Received 28 July 2010; Revised 6 October 2010; Accepted 17 October 2010

KEY WORDS: discrete geometric approach (DGA); cell method (CM); finite integration technique (FIT); complementarity; electrostatics; thick links; (Co)homology

1. INTRODUCTION

A remarkable interest in the techniques for efficient numerical simulation of three-dimensional large-scale electrostatic problems exists. In recent years, for example, the accurate extraction of parasitic circuit parameters for the analysis of the performance and the signal integrity of semiconductor devices and interconnections in integrated circuits (IC) has become fundamental, see for example [1–4]. The strong industrial interest is demonstrated by the number of papers and commercial tools dedicated to this purpose [5–12]. In this context, electromagnetic field solvers play a fundamental role, since they take into account the three-dimensional effects together with the typical multi-layered structures with heterogeneous dielectric material properties and 'floating metal fills', see for example [3, 4, 13, 14]. In recent years, there has been also an increasing interest in solving the Poisson–Schrödinger coupled equations to predict the electronic states in innovative semiconductor devices as quantum dots, see for example [15]. An iterative scheme is frequently

*Correspondence to: Ruben Specogna, Dipartimento di Ingegneria Elettrica, Gestionale e Meccanica (DIEGM), Università di Udine, Via delle Scienze 208, I-33100 Udine, Italy.
†E-mail: ruben.specogna@uniud.it

used to solve this coupled problem [16]. The Poisson solver computes the potential distribution with the knowledge of the electron concentration derived from the Schrödinger solver, until the convergence is reached. Also the accurate evaluation of electrostatic force for the prediction of the mechanical behavior of electrostatic micro electro-mechanical systems (MEMS) requires a number of accurate solutions for large-scale three-dimensional electrostatic boundary value problems (BVPs), see for example [17–19]. The shape optimization of electromagnetic devices—high-voltage insulators for gas-insulated transmission lines [20, 21], just to give an example—or the imaging based on electrical capacitance tomography (ECT) require a considerable computational effort as well. In fact, in these applications, thousands of three-dimensional electrostatic BVPs have to be solved, each time with a different geometry or different parameters of the materials.

Recently, the so-called *Discrete Geometric Approach* (DGA), see for example [22–37], has become an attractive alternative method to solve Maxwell's equations with respect to the widely used finite element method (FEM). Thanks to the exploitation of the topological nature of Maxwell's equations together with the geometric structure behind them [24], the DGA framework presents pedagogical and computational advantages with respect to the widely used FEM. With the DGA, in fact, an algebraic system of equations is directly obtained by combining the physical laws of electromagnetism, enforced exactly by using incidence matrices, together with the constitutive relations, which are approximated on a given mesh by means of the so-called *constitutive matrices* [24]. The constitutive matrices, also called discrete counterparts of the Hodge star operator [31], encode the metric (namely, the geometry of the problem) and the material's parameters.

We would like to mention other methods that try to discretize field theories in different ways: the mimetic discretizations, see for example [38–41], and the mixed-hybrid approaches, see for example [42, 43].

The DGA has already been applied as an efficient numerical method to solve various classes of physical problems ranging from the already discussed electromagnetism to elasticity [44–47]. In particular, to solve electrostatic problems, the formulation based on the electric scalar potential is widely used, see for example [18–21] [24, p. 49–53]. However, it is known that a complementary electrostatic formulation based on a vector potential exists and that the simultaneous use of both formulations has the advantage of providing complementary energy bounds, which allows global quantities—such as capacitance or electrostatic force—to be obtained with high accuracy and minimum computational cost [48–52]. In addition, the use of complementary formulations provide a natural error estimate for adaptive solutions, see for example [53]. Nevertheless, in the literature, little attention is given to the vector potential-based formulation, because it presents theoretical problems in the potential design. In the FEM framework, a formulation based on a vector potential has been presented in [54], where a heuristic solution to the potential design is proposed by introducing appropriate cutting regions. The properties that these regions have to fulfill and how to automatically obtain them are issues left unaddressed in [54].

The aim of this paper is to rigorously introduce a new geometric formulation based on a vector potential by taking advantage of the fundamental tools for the analysis and design of potentials: homology and cohomology theories [55]. A large mathematical literature exists about algebraic topology, which unfortunately is usually far from the theoretical background available to physicists and especially to engineers. For this reason, an informal approach is used in this paper to attract a larger audience. For the sake of brevity, only a minimal description of the essential tools of algebraic topology is included in the paper. The reader not familiar with this topic is invited to consult [56] or [57] for a concise and informal introduction to (co)chain, (co)boundary, and (co)homology. For a more formal presentation, please refer to [55].

The originality of the approach presented in this paper lies in the fact that the design of potentials is tackled directly within a topological setting. In fact, thanks to the reformulation of Maxwell's laws by using incidence matrices, homology and cohomology with integer coefficients are employed for the potential design in place of the standard *de Rham cohomology*, see for example [58]. This approach, although not strictly necessary, presents several advantages. First of all, the integer-based topological solution enables a straightforward development of a graph-theoretic algorithm for the

DOI: 10.1002/nme

automatic potential design. Moreover, new physical insights into the formulation can be presented by exploiting this approach together with the dualities arising when, as in the DGA framework, two interlocked cell complexes—one dual of the other—are employed. For example, using the FEM framework, the so-called *non-local basis functions* have to be added to the set of usual basis functions to be able to span the de Rham second cohomology group. Employing the DGA, the physical interpretation of the non-local basis functions as non-local Faraday's equations becomes apparent.

The paper is structured as follows. In Section 2, the domain of interest of the electrostatic problem and its discrete model are described. The concepts of (co)chain, evaluation of a cochain on a chain, and (co)boundary operator are informally introduced. In Section 3, the electrostatic geometric formulation based on a scalar potential and suitable with a polyhedral mesh is reviewed. In Section 4, the original geometric formulation based on a vector potential and suitable with a polyhedral mesh is introduced by using homology and cohomology theories with integer coefficients. It is shown how a set of the so-called *thick links* is needed to obtain a well-posed BVP. Two algorithms to automatically generate such thick links for a polyhedral cell complex are described. These graph-theoretic algorithms have optimal complexity and are easy to implement. Using these algorithms, cohomology computations by means of the classical Smith Normal Form [55, 59] are avoided, being computationally extremely expensive. Section 5 deals with the reduction of the computational domain in electrostatic problems with symmetries. Section 6 shows how the performances obtained by using both complementary formulations simultaneously largely motivate the investment in the more complicated and time-consuming vector potential formulation. Finally, in Section 7, the conclusions are drawn.

To summarize, the main contributions of the present paper are the following. First, both foundations and technical aspects of complementary geometric formulations for electrostatics suitable with a general polyhedral mesh are rigorously presented. It is shown how the representatives of generators of second cohomology group basis with integer coefficients—called *thick links*—are needed dealing with the formulation based on the vector potential. Finally, two easy-to-implement graph-theoretic algorithms to automatically find such a basis with optimal computational complexity are introduced.

2. DISCRETE MODELS OF THE COMPUTATIONAL DOMAIN AND PHYSICAL VARIABLES

Let us consider a number N_c of conductors $\{\mathscr{C}_i\}_{i=1}^{N_c}$, which are defined as disjoint compact connected subsets of the three-dimensional Euclidean space with connected boundary. Each conductor—which can contain *holes*, see Figure 1(a)—is 'perfect' by hypothesis, meaning that each $\mathscr{C}_i$, and in particular its boundary $\Sigma_i = \partial\mathscr{C}_i$, is equipotential. A set of dielectrics $\{\mathscr{D}_j\}_{j=1}^{N_d}$, composed of materials of permittivities $\{\varepsilon_j\}_{j=1}^{N_d}$, may be present, see Figure 1(a). A permittivity ε_0 is considered in the other regions.

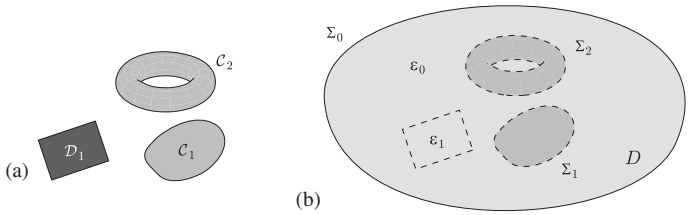

Figure 1. (a) A possible set of conductors $\{\mathscr{C}_i\}_{i=1}^{2}$ involved in an electrostatic problem. The conductor $\mathscr{C}_1$ is topologically trivial, being homeomorphic to the three-dimensional ball. The conductor $\mathscr{C}_2$ is a torus, thus it has a *hole* (the first Betti number β_1 is 1) and (b) The surrounding surface Σ_0 and the domain of interest D for the electrostatic problem.

DOI: 10.1002/nme

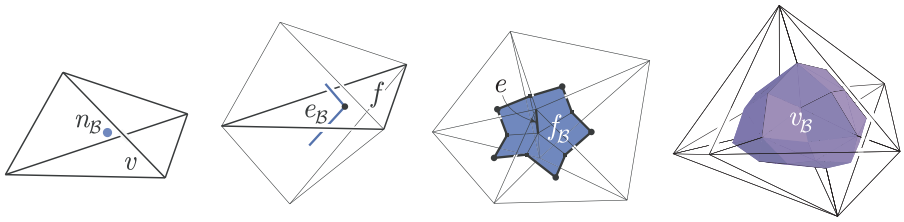

Figure 2. Geometric elements of $\mathscr{K}$ and $\mathscr{B}$ for a simplicial complex $\mathscr{K}$.

The computational domain D is bounded by the surface Σ_0[‡], which contains all the previously defined conductors and dielectrics, see Figure 1(b). In practical problems, the surface Σ_0 is considered to be homeomorphic with a sphere[§].

The domain D is partitioned into a conductive region D_c, formed by $\bigcup_{i=1}^{N_\mathrm{c}} \mathscr{C}_i$, and a dielectric region D_d. The dielectric region D_d is a connected subset of the three-dimensional Euclidean space whose boundary is formed by the union of the N_c connected components $\{\Sigma_i\}_{i=0}^{N_\mathrm{c}}$. Moreover, each conductor represents a cavity for D_d, hence the second Betti number β_2 of D_d is N_c.

2.1. Primal and dual cell complexes

The domain of interest D is covered by a *polyhedral conformal mesh*, whose incidences are encoded in the *cell complex* $\mathscr{K}$ [24–30]. It is assumed that the generated mesh reflects the topology of the domain of interest, i.e. the mesh is adequately refined in such a way that all topological features of D are captured. The subcomplexes of $\mathscr{K}$ relative to geometric elements belonging to the conducting and dielectric regions are denoted by $\mathscr{K}_\mathrm{c}$ and $\mathscr{K}_\mathrm{d}$, respectively. A dual barycentric complex $\mathscr{B}$ is obtained from $\mathscr{K}$ by using the *barycentric subdivision* [27], [56, Section 3]. The elements of $\mathscr{K}$ are denoted by n for a node, e for an edge, f for a face, and v for a cell, whereas the geometric elements of the barycentric complex $\mathscr{B}$ are denoted by $n_{\mathscr{B}}$, $e_{\mathscr{B}}$, $f_{\mathscr{B}}$, and $v_{\mathscr{B}}$, respectively, see Figure 2. The *incidence matrices* [27] specify how the oriented nodes, edges, faces, and cells of the cell complex $\mathscr{K}$ are connected. The incidence matrix between edges and nodes is called $\mathbf{G}$. By $\mathbf{C}$ the incidence matrix between faces and edges is denoted and by $\mathbf{D}$ the incidence matrix between cells and faces. As there is a one-to-one correspondence between a geometric element of dimension d in $\mathscr{K}$ and a geometric element of dimension $3-d$ in $\mathscr{B}$, the matrices $\tilde{\mathbf{G}}=\mathbf{D}^\mathrm{T}$, $\tilde{\mathbf{C}}=\mathbf{C}^\mathrm{T}$, and $\tilde{\mathbf{D}}=-\mathbf{G}^\mathrm{T}$ represent the incidence matrices of the dual barycentric complex [27], [56, Section 3].

2.2. Useful tools from algebraic topology

A *k-chain* [27, 55] with integer coefficients in a cell complex $\mathscr{K}$ is a formal integer combination of all oriented k-dimensional cells in the considered cell complex

$$c=\sum_{S_i^k\in\mathscr{K}} a_i S_i^k, \quad a_i\in\mathbb{Z}, \tag{1}$$

where S_i^k denotes the ith k-dimensional cell in $\mathscr{K}$. k-chains are added by adding the corresponding coefficients. The set of all k-chains in $\mathscr{K}$ form a group with addition called the kth chain group

[‡]If an interior BVP is considered, Σ_0 usually represents the inner surface of a conductive shell. If an exterior BVP is considered, Σ_0 represents a non-physical surface introduced to artificially limit the extent of the computational domain. In the latter case, the surface Σ_0 is supposed to be placed far enough with respect to the conductors, in such a way that a zero potential over such a surface approximates the regularity condition of the scalar potential at infinity. The regularity condition, in fact, prescribes that the potential approaches zero when the distance from the sources tends to infinity. More sophisticated techniques, which are extensively described in the literature, may be used to solve exterior BVP. The most efficient technique is probably to map the infinity at a finite distance through a geometrical transformation, see [60].

[§]For problems arising when more complicated domains of interest D are considered, see [61].

DOI: 10.1002/nme

$C_k(\mathscr{K})$. It is straightforward to see that the set of all k-dimensional cells with a chosen orientation form a basis of $C_k(\mathscr{K})$ [55, p. 28], hence every element of $C_k(\mathscr{K})$ can be obtained in a unique way as an integer combination of the k-dimensional cells. In this paper, let us suppose that the orientation of all the cells is fixed. Then, an arbitrary chain can be represented by an integer array having the corresponding coefficients $\{a_i\}$ as entries. The *support* $|c|$ of $c \in C_k(\mathscr{K})$ is defined as the set of k-dimensional cells with non-zero coefficient: $|c| = \{S_i^k \in \mathscr{K} | a_i \neq 0\}$. A k-dimensional cell S_i^k is a particular case of k-chain—called *elementary k-chain*—whose coefficients are $a_i = 1$ and $a_j = 0, \forall j \neq i$. In the paper, by abuse of notation, we denote—for example—by the edge e not only the oriented one-dimensional cell, but also the corresponding elementary 1-chain.

A *k-cochain* [27, 55] with coefficients in the group $G \in \{\mathbb{Z}, \mathbb{R}\}$ is a linear map $\mathbf{d}: C_k(\mathscr{K}) \to G$. Also cochains can be added and the group of all k-cochains of the complex $\mathscr{K}$ is called k-cochain group $C^k(\mathscr{K}, G)$. For each k-dimensional cell S_i^k, let us define the map $d^{S_i^k}: C_k(\mathscr{K}) \to G$, such that $d^{S_i^k}(S_i^k) = 1$ and $d^{S_i^k}(S_j^k) = 0$ for $j \neq i$. This set of maps, called *elementary k-cochains*, forms a basis [55, p. 252] of $C^k(\mathscr{K}, G)$ which is dual with respect to the standard basis chosen for the chains. It is worth noting that, due to the bijective correspondence between the standard bases of $C_k(\mathscr{K})$ and $C^k(\mathscr{K}, G)$, a one-to-one[¶] correspondence between a chain and a cochain exists. Similarly to the chains, an arbitrary cochain can be expressed as a combination of the basis with coefficients in G

$$\mathbf{d} = \sum_{S_i^k \in \mathscr{K}} b_i d^{S_i^k}, \quad b_i \in G. \tag{2}$$

If $\mathbb{Z}$ is assumed as the group G, the cochain can be represented by an integer array, whereas if the group $\mathbb{R}$ is chosen, the cochain can be represented by a real-valued array. In the latter case, the cochain is called real-valued. In the following, if the group is not explicitly specified, the group of reals is assumed.

Lemma 1
The *evaluation* $\langle \mathbf{d}, c \rangle$ of a k-cochain $\mathbf{d} = \sum_{S_i^k \in \mathscr{K}} b_i d^{S_i^k} \in C^k(\mathscr{K}, G)$ on a k-chain $c = \sum_{S_i^k \in \mathscr{K}} a_i S_i^k \in C_k(\mathscr{K})$ is the value

$$\langle \mathbf{d}, c \rangle = \sum_{S_i^k \in \mathscr{K}} b_i a_i. \tag{3}$$

Proof
$\langle \mathbf{d}, c \rangle = \langle \mathbf{d}, \sum_{S_i^k \in \mathscr{K}} a_i S_i^k \rangle = \sum_{S_i^k \in \mathscr{K}} a_i \langle \mathbf{d}, S_i^k \rangle = \sum_{S_i^k \in \mathscr{K}} a_i \langle \sum_{S_j^k \in \mathscr{K}} b_j d^{S_j^k}, S_i^k \rangle = \sum_{S_i^k \in \mathscr{K}} \sum_{S_j^k \in \mathscr{K}} (a_i b_j \langle d^{S_j^k}, S_i^k \rangle) = \sum_{S_i^k \in \mathscr{K}} \sum_{S_j^k \in \mathscr{K}} (a_i b_j \delta_{ij}) = \sum_{S_i^k \in \mathscr{K}} (a_i b_i)$, where δ_{ij} is the Kronecker delta. □

Given a k-dimensional cell of $\mathscr{K}$, its boundary is a $(k-1)$-chain that can be found by using the information contained in the corresponding incidence matrix. Then, after that the boundary has been defined on the standard basis of $C_k(\mathscr{K})$, the *boundary operator* $\partial: C_k(\mathscr{K}) \to C_{k-1}(\mathscr{K})$ is extended to a chain $c \in C_k(\mathscr{K})$ by linearity

$$\partial c = \partial \sum_{S_i^k \in \mathscr{K}} a_i S_i^k = \sum_{S_i^k \in \mathscr{K}} a_i \partial S_i^k.$$

In addition, one can verify that $\partial \circ \partial c = 0, \forall c \in C_k(\mathscr{K})$, holds. As the boundary operator is a linear map between $C_k(\mathscr{K})$ and $C_{k-1}(\mathscr{K})$ and the bases for $C_k(\mathscr{K})$ and $C_{k-1}(\mathscr{K})$ are fixed, it can be represented as a matrix, which turns out to be the transpose of the corresponding incidence matrix [27].

[¶]Formally, the chain and cochain groups are isomorphic: $C_p(\mathscr{K}) \cong C^p(\mathscr{K})$.

DOI: 10.1002/nme

The *coboundary operator* $\delta: C^k(\mathscr{K}) \to C^{k+1}(\mathscr{K})$ can be defined as dual with respect to the boundary operator by means of the Generalized Stokes Theorem

$$\langle \delta \mathbf{d}, c \rangle = \langle \mathbf{d}, \partial c \rangle. \tag{4}$$

Since the dual standard bases are used, matrices representing dual operators are one the transpose of the other, hence the coboundary operator is represented by the corresponding incidence matrix [27].

2.3. Degrees of freedom

Physical variables can be modeled by real-valued cochains, see for example [27]. Their coefficients, usually called *Degrees of Freedom* (DoFs), are defined by using the so-called *de Rham map* [62]. They are the integrals of electromagnetic scalar and vector fields on oriented geometric elements of the pair of cell complexes $\mathscr{K}$ and $\mathscr{B}$.

For example, the 1-cochain voltage $\mathbf{U}$ can be represented by a real-valued array of DoFs, one DoF for each edge of the considered complex. The DoF $\langle \mathbf{U}, e \rangle$—the voltage associated with the edge e—is defined by using the de Rham map as the integral of the electric field E on the edge e

$$\langle \mathbf{U}, e \rangle = \int_e \mathrm{E} \cdot t \, \mathrm{d}l.$$

3. SCALAR POTENTIAL FORMULATION

3.1. Choice of DoFs and their association

According to the Tonti's classification of physical variables [24], there is a unique association between a physical variable and the corresponding oriented geometric element.

In order to formulate an electrostatic BVP by using the scalar potential formulation, the following DoFs are introduced, see Figure 3:

- *Voltage* $\langle \mathbf{U}, e \rangle$, associated with all $e \in \mathscr{K}_\mathrm{d}$;
- *Electric flux* $\langle \mathbf{\Psi}, f_\mathscr{B} \rangle$, associated with all $f_\mathscr{B} \in \mathscr{B}_\mathrm{d}$;
- *Induced electric charge* $\langle \mathbf{Q}, v_\mathscr{B} \rangle$, associated with all $v_\mathscr{B}$ one-to-one with $n \in \partial \mathscr{K}_\mathrm{d}$;
- *Source electric charge* $\langle \mathbf{Q}_\mathrm{s}, v_\mathscr{B} \rangle$, associated with all $v_\mathscr{B}$ one-to-one with $n \in \mathscr{K}_\mathrm{d} / \partial \mathscr{K}_\mathrm{d}$;
- *Electric scalar potential* $\langle \mathbf{V}, n \rangle$, associated with all $n \in \mathscr{K}_\mathrm{d}$.

The electric field E is known to be zero inside the conductors. For this reason, the cochains are defined in the subcomplex $\mathscr{K}_\mathrm{d}$ only.

3.2. Definition of the scalar potential $\mathbf{V}$ and related formulation

In electrostatics, the electric field E is curl-free by definition. Hence, Faraday's law, in the discrete setting, translates into

$$\langle \mathbf{C}_\mathrm{d} \mathbf{U}, f \rangle = \langle \mathbf{U}, \partial f \rangle = 0 \quad \forall f \in \mathscr{K}_\mathrm{d}. \tag{5}$$

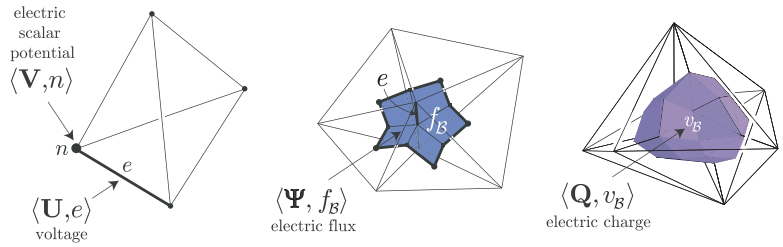

Figure 3. Association of the DoFs with the oriented geometric elements.

DOI: 10.1002/nme

Let us denote by the subscript d the incidence matrices relative to geometrical elements belonging to the subcomplex $\mathscr{K}_{\mathrm{d}}$. The algebraic constraints (5) on the voltages are enforced implicitly by using the electric scalar potential $\mathbf{V}$

$$\mathbf{U} = -\mathbf{G}_{\mathrm{d}}\mathbf{V}, \tag{6}$$

since $\mathbf{C}_{\mathrm{d}}\mathbf{G}_{\mathrm{d}} = \mathbf{0}$ holds.

The discrete counterpart of the electric constitutive relation $\mathrm{D} = \varepsilon\,\mathrm{E}$—the *permittivity constitutive matrix* $\mathbf{E}$ [24]—links the array of voltages $\mathbf{U}$ with the array of electric fluxes $\mathbf{\Psi}$ as

$$\mathbf{\Psi} = \mathbf{E}\mathbf{U}. \tag{7}$$

The permittivity constitutive matrix $\mathbf{E}$ encodes both the information about the material's properties and the metric. It is constructed in such a way that (7) holds for an element-wise uniform electric field E and electric flux density D in each polyhedron and a permittivity ε assumed element-wise constant.

Classical ways to construct $\mathbf{E}$ for a tetrahedral mesh are the Discrete Hodge techniques based on Whitney's maps, described in [31] and [63], or the so-called Galerkin Hodge [64], which is a reinterpretation of FEM with edge element basis functions. Another original solution is to use the piecewise-uniform edge and face vector basis functions defined in [65] for tetrahedra and triangular prisms. As proven in [65], these basis functions assure that symmetry, positive-definiteness, and consistency[‖] properties are satisfied for these constitutive matrices.

Since in this paper a formulation suitable for a general *polyhedral mesh* is sought, the symmetric, positive-definite, and consistent constitutive matrices described in [66] are used (alternatively, one can use that described in [67]). The possibility of using general polyhedral elements, enables the rigorous use of *subgridding* [68]. These constitutive matrices can be constructed by using only the vectors associated with the geometric elements of the cell complexes $\mathscr{K}$ and $\mathscr{B}$, which yields to simple and computationally efficient solutions.

Gauss's balance law is enforced by means of the following algebraic constraints:

$$\begin{aligned} &\langle \tilde{\mathbf{D}}_{\mathrm{d}}\mathbf{\Psi}, v_{\mathscr{B}}\rangle = \langle -\mathbf{G}_{\mathrm{d}}^{\mathrm{T}}\mathbf{\Psi}, v_{\mathscr{B}}\rangle = \langle \mathbf{Q}_s, v_{\mathscr{B}}\rangle \quad \forall v_{\mathscr{B}} \text{ dual to } n \in \mathscr{K}_{\mathrm{d}}/\partial\mathscr{K}_{\mathrm{d}}, \\ &\langle \tilde{\mathbf{D}}_{\mathrm{d}}\mathbf{\Psi}, v_{\mathscr{B}}\rangle = \langle -\mathbf{G}_{\mathrm{d}}^{\mathrm{T}}\mathbf{\Psi}, v_{\mathscr{B}}\rangle = \langle \mathbf{Q}, v_{\mathscr{B}}\rangle \quad \forall v_{\mathscr{B}} \text{ dual to } n \in \partial\mathscr{K}_{\mathrm{d}}. \end{aligned} \tag{8}$$

By substituting (7) and (6) in (8), the following algebraic linear system of equations, having the scalar potentials $(\mathbf{V})_n$ in the nodes $n \in \mathscr{K}_{\mathrm{d}}$ as unknowns, is obtained

$$\begin{aligned} &\langle \mathbf{K}, v_{\mathscr{B}}\rangle\mathbf{V} = \langle \mathbf{Q}_{\mathrm{s}}, v_{\mathscr{B}}\rangle \quad \forall v_{\mathscr{B}} \text{ dual to } n \in \mathscr{K}_{\mathrm{d}}/\partial\mathscr{K}_{\mathrm{d}}, \\ &\langle \mathbf{K}, v_{\mathscr{B}}\rangle\mathbf{V} = \langle \mathbf{Q}, v_{\mathscr{B}}\rangle \quad \forall v_{\mathscr{B}} \text{ dual to } n \in \partial\mathscr{K}_{\mathrm{d}}, \end{aligned} \tag{9}$$

where $\mathbf{K} = \mathbf{G}_{\mathrm{d}}^{\mathrm{T}}\mathbf{E}\mathbf{G}_{\mathrm{d}}$. The equations relative to $v_{\mathscr{B}}$ one-to-one with $n \in \partial\mathscr{K}_{\mathrm{d}}$ depend on the desired boundary conditions. This issue is the subject of Section 3.3.

The process of forming the final algebraic linear system of equations can be conveniently visualized by using Tonti's diagram [24, p. 52] for electrostatics, represented in Figure 4(b). Following the path 1-2-3-4 in the diagram, the equations are derived.

3.3. Non-local quantities and boundary conditions

3.3.1. Dirichlet boundary conditions. Let us call by $\{V_{\mathrm{c}}^i\}_{i=1}^{N_{\mathrm{c}}}$ and $\{Q_{\mathrm{c}}^i\}_{i=1}^{N_{\mathrm{c}}}$ the electric scalar potential and the charge supported by each conductor $\{\mathscr{C}_i\}_{i=1}^{N_{\mathrm{c}}}$, respectively. The potential and the electric

[‖] A precise definition of the notion of consistency for constitutive matrices is given in [33].

DOI: 10.1002/nme

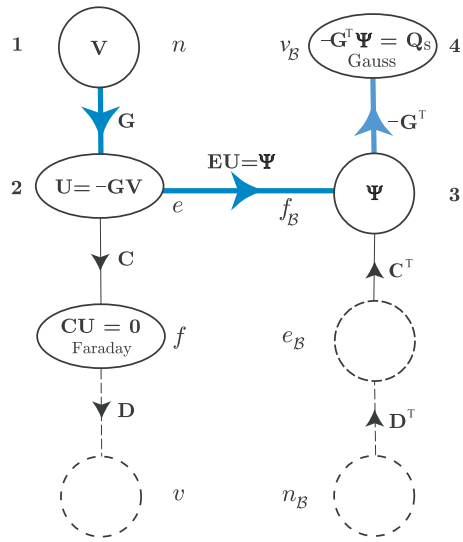

Figure 4. Tonti's diagram for the electrostatic formulation in terms of **V**.

charge associated with the conducting shell Σ_0 are denoted by V_{c}^0 and Q_{c}^0, respectively. Let us fix the potential V_{c}^0 to zero. Each conductive region is equipotential by hypothesis, hence the resulting electric field E will result orthogonal to the conductor's boundaries.

To define a consistent excitation for the electrostatic BVP, a set of N_{c} of independent non-local quantities have to be fixed. In practice, the typical situation is to fix, for each conductor, its potential or alternatively its charge. If the value of the potential V_{c}^i is fixed, the corresponding value can be imposed on all nodes $n \in \Sigma_i$ by means of the Dirichlet boundary conditions. On the contrary, if the conductor $\mathscr{C}_i$ is *isolated*—meaning that $\mathscr{C}_i$ is not connected to any electrical generator—V_{c}^i is an unknown of the electrostatic problem, since V_{c}^i can 'float'. This is the reason why this kind of constraint is usually called *floating potential constraint*. What has to be fixed in this case is the electric charge Q_{c}^i supported by the conductive region $\mathscr{C}_i$.

Let us suppose that the potential of the first N conductors is known, whereas the others are subject to floating potential constraint. Let us order the node's labels in such a way that the nodes $n \in \mathscr{K}_{\mathrm{d}}/\partial\mathscr{K}_{\mathrm{d}}$ come first, followed by the nodes $n \in \bigcup_{j=0}^{N} \Sigma_j$, and finally by the nodes $n \in \bigcup_{k=N+1}^{N_{\mathrm{c}}} \Sigma_k$. Consequently, the array **V** is partitioned into three subarrays $\mathbf{V}'$, $\bar{\mathbf{V}}$, and $\mathbf{V}''$, whether the nodes belong to $\mathscr{K}_{\mathrm{d}}/\partial\mathscr{K}_{\mathrm{d}}$, $\bigcup_{j=0}^{N} \Sigma_j$ or to $\bigcup_{k=N+1}^{N_{\mathrm{c}}} \Sigma_k$, respectively. By partitioning the matrix **K** and the array **Q** accordingly, the linear system of equations can be written as

$$\begin{bmatrix} \mathbf{K}_{11} & \mathbf{K}_{12} & \mathbf{K}_{13} \\ \mathbf{K}_{21} & \mathbf{K}_{22} & \mathbf{K}_{23} \\ \mathbf{K}_{31} & \mathbf{K}_{32} & \mathbf{K}_{33} \end{bmatrix} \begin{bmatrix} \mathbf{V}' \\ \bar{\mathbf{V}} \\ \mathbf{V}'' \end{bmatrix} = \begin{bmatrix} \mathbf{Q}_{\mathrm{s}} \\ \bar{\mathbf{Q}} \\ \mathbf{Q}'' \end{bmatrix}. \tag{10}$$

The values of the potentials in $\bar{\mathbf{V}}$ are known and they can be substituted into (10) and moved on the right-hand side. The equations corresponding to the nodes $n \in \bigcup_{j=0}^{N} \Sigma_j$ are not needed to solve the problem, but they may be used in the post-processing stage to compute the charges induced on the first N conductors with (20). Hence, the system becomes

$$\begin{bmatrix} \mathbf{K}_{11} & \mathbf{K}_{13} \\ \mathbf{K}_{31} & \mathbf{K}_{33} \end{bmatrix} \begin{bmatrix} \mathbf{V}' \\ \mathbf{V}'' \end{bmatrix} = \begin{bmatrix} \mathbf{Q}_{\mathrm{s}} \\ \mathbf{Q}'' \end{bmatrix} - \begin{bmatrix} \mathbf{K}_{12} \\ \mathbf{K}_{32} \end{bmatrix} \bar{\mathbf{V}}. \tag{11}$$

DOI: 10.1002/nme

Let us introduce a family of column arrays $\{\mathbf{n}_i\}_{i=0}^{N_c}$ such that the array $\bar{\mathbf{V}}$ relative to the known potentials can be obtained by

$$\bar{\mathbf{V}} = \sum_{j=0}^{N} V_c^j \, \mathbf{n}_j, \tag{12}$$

whereas the array $\mathbf{V}''$ relative to the floating unknown potentials can be obtained by

$$\mathbf{V}'' = \sum_{k=N+1}^{N_c} V_c^k \, \mathbf{n}_k. \tag{13}$$

Hence, for $i = 0, ..., N$, the array $\mathbf{n}_i$ can be defined as

$$\begin{aligned} &\langle \mathbf{n}_i, n \rangle = 1 \quad \forall n \in \Sigma_i \\ &\langle \mathbf{n}_i, n \rangle = 0 \quad \forall n \in \bigcup_{j=0, j\neq i}^{N} \Sigma_j, \end{aligned} \tag{14}$$

and for $i = N+1, ..., N_c$ as

$$\begin{aligned} &\langle \mathbf{n}_i, n \rangle = 1 \quad \forall n \in \Sigma_i \\ &\langle \mathbf{n}_i, n \rangle = 0 \quad \forall n \in \bigcup_{k=N+1, k\neq i}^{N_c} \Sigma_k. \end{aligned} \tag{15}$$

By using the arrays just defined, the system can be written as

$$\begin{aligned} \mathbf{K}_{11} \, \mathbf{V}' + \sum_{k=N+1}^{N_c} (\mathbf{K}_{13} \, \mathbf{n}_k) \, V_c^k &= \mathbf{Q}_s - \sum_{j=0}^{N} (\mathbf{K}_{12} \, \mathbf{n}_j) \, V_c^j, \\ \mathbf{K}_{31} \, \mathbf{V}' + \sum_{k=N+1}^{N_c} (\mathbf{K}_{33} \, \mathbf{n}_k) \, V_c^k &= \mathbf{Q}'' - \sum_{j=0}^{N} (\mathbf{K}_{32} \, \mathbf{n}_j) \, V_c^j, \end{aligned} \tag{16}$$

where the potentials $\{V_c^k\}_{k=N+1}^{N_c}$ are used as unknowns in place of the DoFs $\mathbf{V}''$ relative to nodes $n \in \bigcup_{k=N+1}^{N_c} \Sigma_k$.

In (16), there are more equations than unknowns, but the equations relative to the nodes $n \in \bigcup_{k=N+1}^{N_c} \Sigma_k$ can be grouped into buckets relative to conductors $k \in \{N+1, ..., N_c\}$ pre-multiplying by $\{\mathbf{n}_k^T\}_{k=N+1}^{N_c}$,

$$(\mathbf{n}_k^T \mathbf{K}_{31}) \mathbf{V}' + (\mathbf{n}_k^T \mathbf{K}_{33} \, \mathbf{n}_k) V_c^k = \mathbf{n}_k^T \mathbf{Q}'' - \sum_{j=0}^{N} (\mathbf{n}_k^T \mathbf{K}_{32} \, \mathbf{n}_j) \, V_c^j, \quad k = N+1, \ldots, N_c, \tag{17}$$

where $\mathbf{n}_k^T \, \mathbf{Q}'' = Q_c^k$. We note that, in practical problems, a mesh is very likely to be refined in such a way that two conductors are separated by much more than just one layer of three-dimensional cells. With this assumption, $(\mathbf{n}_k^T \mathbf{K}_{32} \, \mathbf{n}_j) = 0$, $\forall k \in \{N+1, \ldots, N_c\}$ and $\forall j \in \{1, \ldots, N\}$.

The final symmetric linear system of equations becomes

$$\begin{aligned} \mathbf{K}_{11} \, \mathbf{V}' + \sum_{k=N+1}^{N_c} (\mathbf{K}_{13} \, \mathbf{n}_k) \, V_c^k &= \mathbf{Q}_s - \sum_{j=0}^{N} (\mathbf{K}_{12} \, \mathbf{n}_j) \, V_c^j, \\ (\mathbf{n}_k^T \mathbf{K}_{31}) \mathbf{V}' + (\mathbf{n}_k^T \mathbf{K}_{33} \, \mathbf{n}_k) V_c^k &= Q_c^k, \quad k = N+1, \ldots, N_c. \end{aligned} \tag{18}$$

The electric scalar potential in all the nodes $n \in \mathscr{K}_d$ can be recovered in the post-processing stage by using

$$\begin{aligned} &\langle \mathbf{V}, n \rangle = \langle \mathbf{V}', n \rangle \quad \forall n \in \mathscr{K}_d / \partial \mathscr{K}_d \\ &\langle \mathbf{V}, n \rangle = V_c^i \quad \forall n \in \Sigma_i, i = 0, \ldots, N_c. \end{aligned} \tag{19}$$

DOI: 10.1002/nme

The charges induced on the conductors $\{\mathscr{C}_j\}_{j=0}^{N}$ can be computed with

$$Q_{\mathrm{c}}^{j} = \mathbf{n}_j^{\mathrm{T}}(\mathbf{K}_{21}\mathbf{V}' + \mathbf{K}_{22}\bar{\mathbf{V}} + \mathbf{K}_{23}\mathbf{V}''), \quad j = 0, \ldots, N. \tag{20}$$

The formulation presented in (18) is different from the well-known technique of treating the floating potential constraint in the corresponding FEM formulation [69]. In fact, the approach used in the FEM electrostatic formulation, recalled also in [70], is based on the definition of non-local nodal basis functions. In this paper, nodal basis functions are not used at all, and the floating potential constraint is imposed by using only the topological information contained in the integer-valued arrays $\mathbf{n}_i$, enabling a straightforward implementation.

4. VECTOR POTENTIAL FORMULATION

4.1. Choice of DoFs and their association

In order to formulate an electrostatic BVP by using the vector potential formulation, the DoFs are associated with the geometrical elements dually with respect to that introduced in the scalar potential formulation, see Figure 5:

- *Voltage* $\langle \mathbf{U}, e_{\mathscr{B}} \rangle$, associated with all $e_{\mathscr{B}} \in \mathscr{B}$;
- *Electric flux* $\langle \mathbf{\Psi}, f \rangle$, associated with all $f \in \mathscr{K}$;
- *Induced electric charge* $\langle \mathbf{Q}, v \rangle$, associated with all $v \in \mathscr{K}_{\mathrm{c}}$;
- *Source electric charge* $\langle \mathbf{Q}_{\mathrm{s}}, v \rangle$, associated with all $v \in \mathscr{K}_{\mathrm{d}}$;
- *Electric vector potential* $\langle \mathbf{P}, e \rangle$, associated with all $e \in \mathscr{K}_{\mathrm{d}}$.

4.2. Potential design

If one introduces an electric vector potential $\mathbf{P}$ by using the preliminary definition

$$\mathbf{\Psi} = \mathbf{C}\mathbf{P}, \tag{21}$$

since $\mathbf{D}\mathbf{C} = \mathbf{0}$, the following inconsistency in the Gauss's law holds $\mathbf{D}\mathbf{\Psi} = \mathbf{D}\mathbf{C}\mathbf{P} = \mathbf{0} \neq \mathbf{Q}_{\mathrm{s}}$. A similar inconsistency due to the induced charges exists. To solve these inconsistencies, there is the need to modify the definition of potential (21) in such a way that Gauss's law holds implicitly in $\mathscr{K}_{\mathrm{d}}$. In the following, to solve this issue, we take advantage of a branch of algebraic topology called *cohomology theory*, see for example [55, 56]. In Section 4.2.1 we describe how to fix the inconsistency due to source charges, in Section 4.2.2 a minimal introduction to (co)homology is provided, and in Section 4.2.3 the focus is given on fixing the inconsistency due to induced charges.

4.2.1. Taking into account source electric charges. The source charges can be taken into account by constructing a 2-cochain $\mathbf{S}$ such that

$$\langle \mathbf{D}\mathbf{S}, v \rangle = \langle \mathbf{S}, \partial v \rangle = \langle \mathbf{Q}_{\mathrm{s}}, v \rangle \tag{22}$$

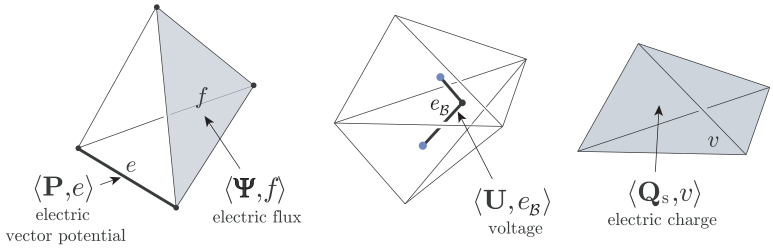

Figure 5. Association of the DoFs with the oriented geometric elements.

DOI: 10.1002/nme

and by defining

$$\mathbf{\Psi} = \mathbf{CP} + \mathbf{S}. \tag{23}$$

By using (23), Gauss's law holds implicitly since $\mathbf{D\Psi} = \mathbf{D}(\mathbf{CP}+\mathbf{S}) = \mathbf{DS} = \mathbf{Q}_s$. Of course, $\mathbf{S}$ is not unique. In fact, if two 2-cochains $\mathbf{S}_1$ and $\mathbf{S}_2$ differ by the coboundary of a 1-cochain $\mathbf{R}$, then $\mathbf{DS}_1 = \mathbf{D}(\mathbf{S}_2 + \mathbf{CR}) = \mathbf{DS}_2$ holds. An efficient technique to build a 2-cochain $\mathbf{S}$ that satisfies (22) is described in Section 4.5.

4.2.2. (*Co*)*homology theory in brief.* The boundary operator gives rise to a classification of chains. k-chains whose boundary is zero belong to the *cycles group* of $\mathscr{K}$, denoted as $Z_k(\mathscr{K})$. k-chains, which are boundary of a $(k+1)$-chain, belong to the *boundary group* of $\mathscr{K}$, denoted by $B_k(\mathscr{K})$. Elements of $Z_k(\mathscr{K})$ are called *k-cycles* and elements of $B_k(\mathscr{K})$ are called *k-boundaries* in $\mathscr{K}$. It is straightforward to convince oneself that all k-boundaries are k-cycles, but the converse is not true. In particular, the *homology group* is defined as the following quotient group:

$$H_k(\mathscr{K}) = Z_k(\mathscr{K})/B_k(\mathscr{K}), k \in \mathbb{N}. \tag{24}$$

Given a cycle z belonging to the kth homology group, adding any k-boundary b to it does not make $z+b$ a boundary. Regarding homology theory, z and $z+b$ are equivalent, which motivates the following equivalence relation. Two k-cycles z_1 and z_2 are *homologous* if their difference is a boundary

$$z_1 \sim z_2 \Leftrightarrow z_1 - z_2 \in B_k(\mathscr{K}).$$

The homology is an equivalence relation that divides the cycles into equivalence classes, which are called *homology classes*. A set of homology classes exist such that any other homology class can be written in a unique way as a combination of these classes with integer coefficients. Such a set of homology classes are referred to as *homology generators*. From homology generators one can generate the whole homology group and the set of all homology generators is called a *homology basis*. Only one representative z from each class is needed, being possible to obtain all other cycles in the class by adding a boundary chain to z. When it is not confusing, for brevity, by homology generators we refer to both the equivalence classes of the presented relation and the cycles that represents the equivalence class.

An analogous classification can be stated regarding the cochains. The group of *k-cocycles* $Z^k(\mathscr{K})$ contains the k-cochains whose coboundary is zero, whereas the group of *k-coboundaries* $B^k(\mathscr{K})$ contains k-cochains which are the coboundary of a $(k-1)$-cochain. The *cohomology group* is the quotient group

$$H^k(\mathscr{K}) = Z^k(\mathscr{K})/B^k(\mathscr{K}), \quad k \in \mathbb{N}, \tag{25}$$

which contains k-cocycles that are not k-coboundaries. It is demonstrated, for example in [55], that the following isomorphisms exist $H_k(\mathscr{K}) \cong H^k(\mathscr{K})$ for complexes embeddable in $\mathbb{R}^3$, which implies that the homology and cohomology generators can be put in one-to-one correspondence.

4.2.3. Taking into account induced electric charges. To focus on induced charges, let us suppose in this section that there are no source charges, hence $\mathbf{Q}_s = \mathbf{0}$. With this assumption, $\mathbf{\Psi}$ has to verify

$$\langle \mathbf{D\Psi}, v \rangle = \langle \mathbf{\Psi}, \partial v \rangle = 0 \quad \forall v \in \mathscr{K}_d. \tag{26}$$

It follows that $\mathbf{\Psi}$ is a 2-cocycle in $\mathscr{K}_d$: $\mathbf{\Psi} \in Z^2(\mathscr{K}_d)$.

Let us analyze now what happens when the Gauss's law is not enforced locally as in (26) (namely on a cell v and its boundary faces), but involve a 3-chain τ—whose support is a set of cells in $\mathscr{K}$—and its boundary 2-cycle $s = \partial\tau$. In particular, let us assume that the support $|s|$ of s is contained in $\mathscr{K}_d$. The resulting Gauss's law, referred to as *non-local*, is written as

$$\langle \mathbf{\Psi}, s \rangle = \langle \mathbf{Q}, \tau \rangle. \tag{27}$$

DOI: 10.1002/nme

If s is a 2-boundary in $\mathscr{K}_{\mathrm{d}}$, the Gauss' law holds even by using the potential $\mathbf{P}$ alone. In fact, the following Lemma holds.

Lemma 2
The evaluation of the 2-cocycle $\mathbf{\Psi} \in Z^2(\mathscr{K}_{\mathrm{d}})$ on a 2-boundary $s \in B_2(\mathscr{K}_{\mathrm{d}})$ is zero.

Proof
As $s \in B_2(\mathscr{K}_{\mathrm{d}})$, there exists a 3-chain $t \in C_3(\mathscr{K}_{\mathrm{d}})$ such that $\partial t = s$. It follows that $\langle \mathbf{\Psi}, s \rangle = \langle \mathbf{\Psi}, \partial t \rangle = \langle \mathbf{D}\mathbf{\Psi}, t \rangle = \langle \mathbf{0}, t \rangle = 0$. □

If the 2-cycle s encircle some conductors, s is not a 2-boundary in $\mathscr{K}_{\mathrm{d}}$, since it cannot be the boundary of any 3-chain in $\mathscr{K}_{\mathrm{d}}$ (but, of course, can be boundary of a 3-chain in $\mathscr{K}$). Hence, s is non-trivial in the second homology group $H_2(\mathscr{K}_{\mathrm{d}})$ with integer coefficients. It is straightforward to see that only the 2-cycles which are non-trivial in the second homology group encircle some conductors and consequently contain a non-zero induced electric charge in general. As we will see, the inconsistency arises only when Gauss's law is applied on this kind of 2-cycles.

Let us now focus on the second homology group $H_2(\mathscr{K}_{\mathrm{d}})$. It is intuitive that a set of independent 2-cycles that do not bound any 3-chain in $\mathscr{K}_{\mathrm{d}}$ is just the set of 2-cycles $\{\Sigma_i\}_{i=1}^{N_{\mathrm{c}}}$**. The number of the second homology group $H_2(\mathscr{K}_{\mathrm{d}})$ generators is the second Betti number $\beta_2(\mathscr{K}_{\mathrm{d}})$, which is the number of cavities N_{c} in $\mathscr{K}_{\mathrm{d}}$. Hence, the 2-chains $\{\Sigma_i\}_{i=1}^{N_{\mathrm{c}}}$ are a maximal set of independent 2-chains and for this reason they can be considered as representatives of generators for the second homology group $H_2(\mathscr{K}_{\mathrm{d}})$. Since this basis is the most natural and no homology computation is needed to obtain it, we refer to this basis as *canonical*. In this paper, we always consider the basis of $H_2(\mathscr{K}_{\mathrm{d}})$ fixed to the canonical one.

Once a basis for $H_2(\mathscr{K}_{\mathrm{d}})$ is given, all possible 2-cycles $c_2 \in Z_2(\mathscr{K}_{\mathrm{d}})$ can be obtained by adding a 2-boundary $b \in B_2(\mathscr{K}_{\mathrm{d}})$ to a linear combination with integer coefficients of the representatives of the homology generators

$$c_2 = \sum_{i=1}^{N_{\mathrm{c}}} a_i \Sigma_i + b, b \in B_2(\mathscr{K}_{\mathrm{d}}), \quad a_i \in \mathbb{Z}. \tag{28}$$

Example 1
As an example, two conductors—a sphere and a torus—are considered. $\mathscr{K}_{\mathrm{d}}$ is the subcomplex obtained as the complement of the two conductors with respect to a big box, which represents the surrounding dielectric domain, see Figure 6. A 2-cycle c that encircle both the conductors can be obtained by adding a 2-boundary $b \in B_2(\mathscr{K}_{\mathrm{d}})$ to $\Sigma_1 + \Sigma_2$. □

The following Lemma holds.

Lemma 3
For two 2-cycles s_1 and s_2 in the same homology class and a 2-cocycle $\mathbf{\Psi}$, $\langle \mathbf{\Psi}, s_1 \rangle = \langle \mathbf{\Psi}, s_2 \rangle$ holds.

Proof
As s_1 and s_2 differ by a 2-boundary, it follows that there exists a 3-chain $t \in C_3(\mathscr{K}_{\mathrm{d}})$ such that $s_1 = s_2 + \partial t$. From (26), it follows that $\langle \mathbf{\Psi}, s_1 \rangle = \langle \mathbf{\Psi}, s_2 + \partial t \rangle = \langle \mathbf{\Psi}, s_2 \rangle + \langle \mathbf{\Psi}, \partial t \rangle = \langle \mathbf{\Psi}, s_2 \rangle$. □

This lemma implies that a precise electric flux evaluation is associated with each homology class of 2-cycles in $\mathscr{K}_{\mathrm{d}}$. The value of such evaluation of $\mathbf{\Psi}$ on the representatives of the homology generators is provided by the non-local Gauss's law

$$\langle \mathbf{\Psi}, \Sigma_i \rangle = Q_{\mathrm{c}}^i, \tag{29}$$

**The 2-cycle Σ_0 has to be excluded, in fact the 2-cycle $T = \bigcup_{j=0}^{N_{\mathrm{c}}} \Sigma_j$ is a 2-boundary, being the boundary of $\mathscr{K}_{\mathrm{d}}$.

DOI: 10.1002/nme

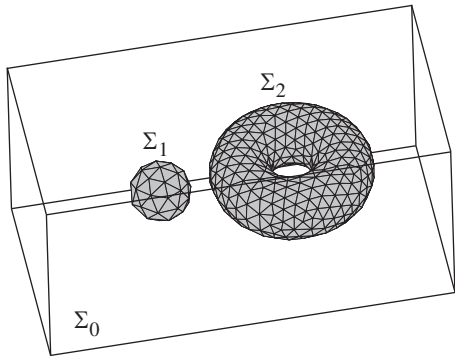

Figure 6. The boundary of $\mathscr{K}_{\mathrm{d}}$ is the union of three connected components: Σ_1, Σ_2, and the boundary of the external box Σ_0 (Σ_0 is only outlined in the figure for the sake of clarity).

where $\{Q_{\mathrm{c}}^i\}_{i=1}^{N_{\mathrm{c}}}$ is the set of *independent electric-induced charges* defined as

$$Q_{\mathrm{c}}^i = \langle \mathbf{Q}, \mathscr{C}_i \rangle. \tag{30}$$

Once the evaluations of the electric flux on the representatives of the homology generators are known, the electric flux $\langle \mathbf{\Psi}, s_2 \rangle$ evaluated on a generic 2-cycle c_2, represented by (28), can be recovered as a linear combination of the $\{Q_{\mathrm{c}}^i\}_{i=1}^{N_{\mathrm{c}}}$ as

$$\langle \mathbf{\Psi}, s_2 \rangle = \sum_{i=1}^{N_{\mathrm{c}}} a_i \langle \mathbf{\Psi}, \Sigma_i \rangle + \langle \mathbf{\Psi}, b \rangle = \sum_{i=1}^{N_{\mathrm{c}}} a_i Q_{\mathrm{c}}^i, b \in B_2(\mathscr{K}_{\mathrm{d}}), \quad a_i \in \mathbb{Z}, \tag{31}$$

where $\langle \mathbf{\Psi}, b \rangle = 0$ for Lemma 2. It is important to note that the integer coefficients $\{a_i\}_{i=1}^{N_{\mathrm{c}}}$ are exactly the same as that in (28).

As indicated by (29), the evaluations of $\mathbf{\Psi}$ over homologically non-trivial 2-chains have to be nonzero in general, and such evaluations cannot be represented by using the coboundary of the vector potential $\mathbf{P}$ only—as in (21)—since it always gives zero evaluation over 2-cycles. To solve this issue, the next theorem is stated.

Theorem 1
A family of integer-valued 2-cochains $\{\mathbf{\Pi}^i\}_{i=1}^{N_{\mathrm{c}}}$ is introduced. Each $\mathbf{\Pi}^i$, called *thick link*[††], has to satisfy the following properties:

1. $\mathbf{\Pi}^i$ is a 2-cocycle in $\mathscr{K}_{\mathrm{d}}$: $\mathbf{\Pi}^i \in Z^2(\mathscr{K}_{\mathrm{d}}, \mathbb{Z})$.
2. Considering the 2-cycles $\{\Sigma_j\}_{j=1}^{N_{\mathrm{c}}}$ that are the representatives of generators for the $H_2(\mathscr{K}_{\mathrm{d}})$ homology group,

$$\langle \mathbf{\Pi}^i, \Sigma_j \rangle = \delta_{ij} \tag{32}$$

holds.

Moreover, the potential definition in (21) is substituted with

$$\mathbf{\Psi} = \mathbf{C}\mathbf{P} + \sum_{i=1}^{N_{\mathrm{c}}} Q_{\mathrm{c}}^i \mathbf{\Pi}^i. \tag{33}$$

Then, the non-local Gauss's law (31) holds for all 2-cycles $c_2 \in Z_2(\mathscr{K}_{\mathrm{d}})$, represented by (28).

[††]The name thick link is borrowed from [71], although its definition is different with respect to that used in this paper. (In [71] a thick link is defined as a set of tetrahedra.)

DOI: 10.1002/nme

Proof

$$\langle \mathbf{\Psi}, c_2 \rangle = \langle \mathbf{CP}, c_2 \rangle + \sum_{i=1}^{N_c} Q_c^i \langle \mathbf{\Pi}^i, c_2 \rangle = \sum_{i=1}^{N_c} Q_c^i \sum_{j=1}^{N_c} a_j \langle \mathbf{\Pi}^i, \Sigma_j \rangle = \sum_{i=1}^{N_c} \sum_{j=1}^{N_c} Q_c^i a_j \delta_{ij} = \sum_{i=1}^{N_c} a_i Q_c^i. \quad (34)$$

□

The following theorem holds.

Theorem 2
The thick links $\{\mathbf{\Pi}^i\}_{i=1}^{N_c}$ are the representatives of generators for the second cohomology group $H^2(\mathscr{K}_d, \mathbb{Z})$.

Proof
One can prove that the set of all thick links form a set of representatives of a cohomology basis by using the Universal Coefficients Theorem, see for example [72]. The authors decided to omit this proof, since it does not give any new light on the practical aspects of the problem. □

Equation (33) shows that the whole 2-cochain group $C^2(\mathscr{K}_d)$ can be spanned by the coboundary of the vector potential $\mathbf{CP} \in B^2(\mathscr{K}_d)$ together with a linear combination of the representatives of the second cohomology group $H^2(\mathscr{K}_d, \mathbb{Z})$ generators using the corresponding induced electric charges as coefficients.

Concretely, the thick links can be represented as arrays of integer coefficients, one coefficient for each face $f \in \mathscr{K}_d$. The coefficients have to fulfill the constraints described in Theorem 1. One possibility is to choose as the support of the thick link the faces dual to dual edges that form a path from each Σ_i to Σ_0. By adopting the same complex used in Example 1, a possible set of thick links constructed by using this technique is shown in Figure 7. Two automatic and efficient algorithms to compute the thick links are presented in Section 4.6.

4.3. Formulation in terms of **P**

Once a family of thick links $\{\mathbf{\Pi}^i\}_{i=1}^{N_c}$ is obtained and a 2-cochain $\mathbf{S}$ representing the source electric charges $\mathbf{Q}_s$ is determined, it is possible to represent a general electric flux 2-cochain $\mathbf{\Psi}$ by using

$$\mathbf{\Psi} = \mathbf{CP} + \mathbf{S} + \sum_{i=1}^{N_c} Q_c^i \mathbf{\Pi}^i. \quad (35)$$

By using (35), Gauss's law holds implicitly for each 2-cycle in $\mathscr{K}_d$, hence the potentials are designed. If the ith conductor is isolated, then the induced charge Q_c^i is known. On the contrary, if the electric potential of the ith conductor is known, Q_c^i is an additional unknown of the problem.

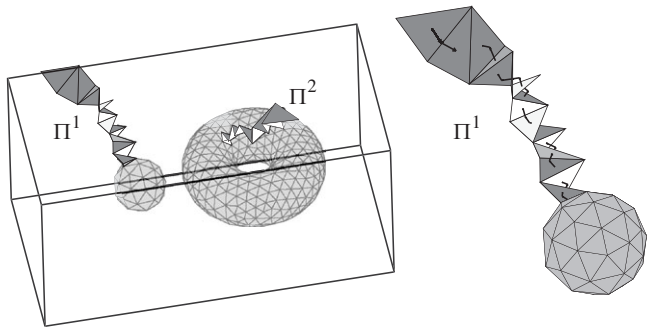

Figure 7. On the left, a family of possible thick links for the Example 1. On the right, the dual edges dual to faces belonging to the support of a thick link form a path on $\mathscr{B}_d$. These paths are used to impose boundary conditions in Section 4.4.3.

DOI: 10.1002/nme

The *inverse permittivity constitutive matrix* links the electric fluxes $\mathbf{\Psi}$ to voltages $\mathbf{U}$

$$\mathbf{U} = \boldsymbol{\eta}\mathbf{\Psi}. \tag{36}$$

$\boldsymbol{\eta}$ is constructed in such a way that (36) holds for an element-wise *uniform* electric field E and electric flux density field D in each polyhedron and it is the approximate discrete counterpart of the constitutive relation $\mathrm{E} = \eta \mathrm{D}$ at continuous level, $\eta = \varepsilon^{-1}$ being the inverse of electrical permittivity assumed element-wise constant. Concerning the construction of $\boldsymbol{\eta}$, the same techniques described for the construction of the permittivity constitutive matrix $\mathbf{E}$ in (7) can be used.

Faraday's balance law,

$$\langle \mathbf{C}^{\mathrm{T}}\mathbf{U}, f_{\mathscr{B}} \rangle = \langle \mathbf{U}, \partial f_{\mathscr{B}} \rangle = 0 \quad \forall f_{\mathscr{B}} \in \mathscr{B}_{\mathrm{d}}, \tag{37}$$

is enforced by a linear system of equations. By substituting (36) and (35) in (37), an algebraic equation is obtained for each dual face $f_{\mathscr{B}} \in \mathscr{B}_{\mathrm{d}}$ as

$$\mathbf{C}^{\mathrm{T}}\boldsymbol{\eta}\mathbf{C}\mathbf{P} + \sum_{j=1}^{N} (\mathbf{C}^{\mathrm{T}}\boldsymbol{\eta}\mathbf{\Pi}^{j}) Q_{\mathrm{c}}^{j} = -\mathbf{C}^{\mathrm{T}}\boldsymbol{\eta}\mathbf{S} - \sum_{k=N+1}^{N_{\mathrm{c}}} (\mathbf{C}^{\mathrm{T}}\boldsymbol{\eta}\mathbf{\Pi}^{k}) Q_{\mathrm{c}}^{k}, \tag{38}$$

where, as in the scalar potential formulation, the conductors $j = 1, \ldots, N$ are associated with a known potential, while the others $k = N+1, \ldots, N_{\mathrm{c}}$ are subject to the floating potential constraint.

The process of forming the linear system of equations can be conveniently visualized by using Tonti's diagram for the formulation in terms of $\mathbf{P}$, represented in Figure 8. Following the path 1-2-3-4 in the diagram, the equations are obtained.

4.4. Non-local quantities and boundary conditions

4.4.1. Dirichlet boundary condition. A Dirichlet boundary condition has to be imposed on the boundaries of conductors, since the boundary of each conductor is equipotential. The electric field E will result normal to the considered surface. This condition is simply imposed by considering the vector potential $\langle \mathbf{P}, e \rangle$ unknown on each edge e belonging to the considered boundary surface. In this case, in fact, Faraday's law (37) is enforced also on a dual face $f_{\mathscr{B}}$ one-to-one with the edge e lying on the considered boundary, see Figure 9(a). As one can see in Figure 9(b), the boundary of $f_{\mathscr{B}}$ also contains the edge l, which lies on the boundary surface. Not considering the contribution of the voltage associated with the line l in Faraday's balance law implicitly enforces this voltage to zero.

4.4.2. Relative homology theory. Relative homology theory [55] is an extension of homology theory suitable to deal with boundary conditions. Given a subcomplex $\mathscr{S}$ of $\mathscr{K}$, a k-chain $z \in C_k(\mathscr{K})$ is a *relative cycle modulo* $\mathscr{S}$, $z \in Z_k(\mathscr{K}, \mathscr{S})$, if $\partial z \in C_{k-1}(\mathscr{S})$. $t \in C_k(\mathscr{K})$ is a *relative boundary modulo* $\mathscr{S}$, $t \in B_k(\mathscr{K}, \mathscr{S})$, if $t = \partial x + y$ for some $x \in C_{k+1}(\mathscr{K})$, $y \in C_k(\mathscr{S})$. The second *relative homology group* $H_2(\mathscr{K}, \mathscr{S})$ is defined as $H_2(\mathscr{K}, \mathscr{S}) = Z_2(\mathscr{K}, \mathscr{S}) / B_2(\mathscr{K}, \mathscr{S})$.

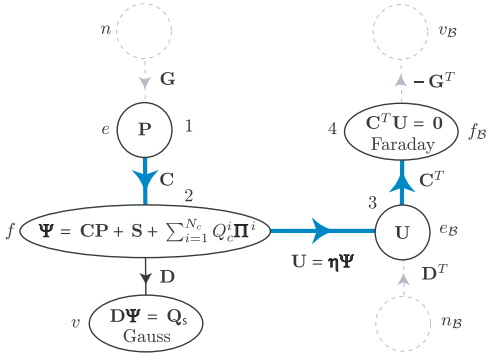

Figure 8. Tonti's diagram for the electrostatic formulation in terms of $\mathbf{P}$.

DOI: 10.1002/nme

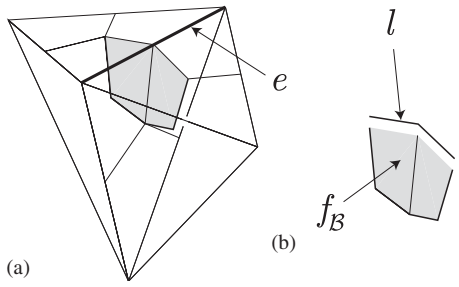

Figure 9. (a) The edge e lies on the boundary. The dual face $f_{\mathcal{B}}$, one-to-one with e, is highlighted. (b) The boundary of $f_{\mathcal{B}}$ contains also the edge l.

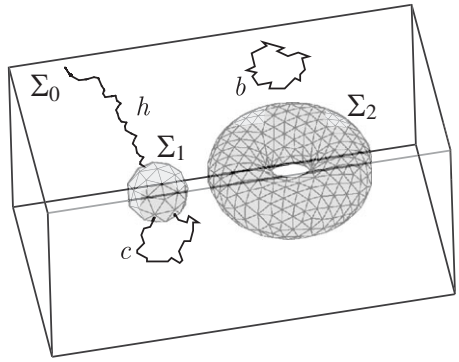

Figure 10. Three 1-chains are defined on the complex $\mathscr{B}_\mathrm{d}$ used in Example 1: $b \in B_1(\mathscr{K}_\mathrm{d})$, $c \in B_1(\mathscr{K}_\mathrm{d}, \partial\mathscr{K}_\mathrm{d})$, and $h \in H_1(\mathscr{K}_\mathrm{d}, \partial\mathscr{K}_\mathrm{d})$.

As a clarifying example, let us concentrate on the complex $\mathscr{B}_\mathrm{d}$ used in Example 1, see Figure 10. Three kinds of 1-chains are present in the figure. The 1-boundary $b \in B_1(\mathscr{B}_\mathrm{d})$ is boundary of a 2-chain $s \in \mathscr{B}_\mathrm{d}$. The 1-chain c is a relative boundary, $c \in B_1(\mathscr{B}_\mathrm{d}, \partial\mathscr{B}_\mathrm{d})$, since the boundary of c lies on $C_0(\partial\mathscr{B}_\mathrm{d})$ and, together with a 1-chain in $\partial\mathscr{B}_\mathrm{d}$, bound a 2-chain $t \in \mathscr{B}_\mathrm{d}$. It is easy to see that this property holds if the boundary nodes of c lie on the same connected component of $\partial\mathscr{B}_\mathrm{d}$. On the contrary, if the boundary nodes of a 1-chain h lie on two different connected components of $\partial\mathscr{B}_\mathrm{d}$, then h together with a 1-chain in $\partial\mathscr{B}_\mathrm{d}$ do not bound any 2-chain in $\mathscr{B}_\mathrm{d}$, see Figure 10. Chains as h are non-trivial in the first relative homology group $H_1(\mathscr{B}_\mathrm{d}, \partial\mathscr{B}_\mathrm{d})$.

Next theorem shows how a basis for $H_1(\mathscr{B}_\mathrm{d}, \partial\mathscr{B}_\mathrm{d})$ can be obtained by exploiting the duality with thick links.

Theorem 3

Let us construct a family of 1-chains $\{\mathbf{\Lambda}_i\}_{i=1}^{N_\mathrm{c}}$ in $\mathscr{B}_\mathrm{d}$, where each element of $\{\mathbf{\Lambda}_i\}_{i=1}^{N_\mathrm{c}}$ is called *link*. The coefficient of the link $\mathbf{\Lambda}_i$ relative to the dual edge $e_{\mathscr{B}}$ is $\langle \mathbf{\Pi}^i, f \rangle$, where the face $f \in \mathscr{K}_\mathrm{d}$ is dual to $e_{\mathscr{B}}$, see Figure 11. The $\{\mathbf{\Lambda}_i\}_{i=1}^{N_\mathrm{c}}$ form a set of representatives for the first relative homology group $H_1(\mathscr{B}_\mathrm{d}, \partial\mathscr{B}_\mathrm{d})$ basis dual to the basis of the second cohomology group $H^2(\mathscr{K}_\mathrm{d}, \mathbb{Z})$ corresponding to the thick links.

Proof

The links, as above defined, are clearly non-trivial elements of $H_1(\mathscr{B}_\mathrm{d}, \partial\mathscr{B}_\mathrm{d})$. The independency can be shown by resorting to the classical Poincaré–Lefschetz duality theorem[‡‡] [55]

$$H^2(\mathscr{K}_\mathrm{d}, \mathbb{Z}) \simeq H_1(\mathscr{B}_\mathrm{d}, \partial\mathscr{B}_\mathrm{d}), \tag{39}$$

which shows that links can be put in one-to-one correspondence with the thick links. □

[‡‡]It is well known that there cannot be *torsion* [55] in the following homology/cohomology groups $H_i(\mathscr{K}_\mathrm{d})$, $H^i(\mathscr{K}_\mathrm{d})$, $H_i(\mathscr{K}_\mathrm{d}, \partial\mathscr{K}_\mathrm{d})$, and $H^i(\mathscr{K}_\mathrm{d}, \partial\mathscr{K}_\mathrm{d})$ for complexes embeddable in $\mathbb{R}^3$.

DOI: 10.1002/nme

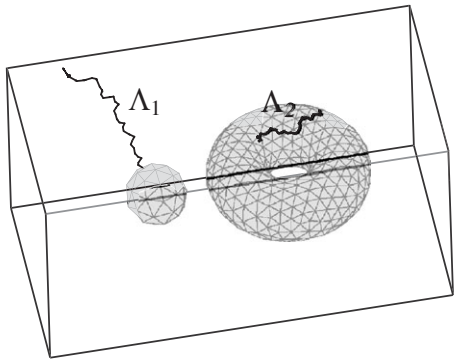

Figure 11. The two links for Example 1. The boundary nodes of each link lie on two different connected components of $\partial\mathscr{B}_\mathrm{d}$.

Every 1-chain $c_1 \in C_1(\mathscr{B}_\mathrm{d})$ can be represented by a linear combination with integer coefficients of the links plus a relative boundary $c \in B_1(\mathscr{B}_\mathrm{d}, \partial\mathscr{B}_\mathrm{d})$

$$c_1 = \sum_{i=1}^{N_\mathrm{c}} b_i \, \mathbf{\Lambda}_i + c, c \in B_1(\mathscr{B}_\mathrm{d}, \partial\mathscr{B}_\mathrm{d}), \quad b_i \in \mathbb{Z}. \tag{40}$$

4.4.3. Independent voltages and non-local Faraday's laws. If Faraday's law is applied on a 1-boundary $b \in B_1(\mathscr{B}_\mathrm{d})$ or on a 1-chain $c \in B_1(\mathscr{B}_\mathrm{d}, \partial\mathscr{B}_\mathrm{d})$ which is a relative boundary, see Figure 10, the evaluation of $\mathbf{U}$ is zero. In fact

$$\langle \mathbf{CU}, s \rangle = \langle \mathbf{0}, s \rangle = 0, \tag{41}$$

where $b = \partial s$ or $c + t = \partial s$, $t \in \partial\mathscr{B}_\mathrm{d}$.

The voltage on a general 1-chain $c_1 \in C_1(\mathscr{B}_\mathrm{d})$ can be obtained by using the same coefficients as the linear combination in (40) as

$$\langle \mathbf{U}, c_1 \rangle = \sum_{i=1}^{N_\mathrm{c}} b_i \langle \mathbf{U}, \mathbf{\Lambda}_i \rangle + \langle \mathbf{U}, c \rangle = \sum_{i=1}^{N_\mathrm{c}} b_i U_\mathrm{c}^i, c \in B_1(\mathscr{B}_\mathrm{d}, \partial\mathscr{B}_\mathrm{d}), b_i \in \mathbb{Z}, \tag{42}$$

where the voltages evaluated over the links represent a set of *independent voltages* $\{U_\mathrm{c}^j\}_{j=1}^{N_\mathrm{c}}$ defined as

$$U_\mathrm{c}^i = \langle \mathbf{U}, \mathbf{\Lambda}_i \rangle. \tag{43}$$

The final algebraic linear system of Equations (38) contains one equation for each edge in $\mathscr{K}_\mathrm{d}$. Nonetheless, it contains as unknowns, in addition to the vector potential $\langle \mathbf{P}, e \rangle$ on all edges $e \in \mathscr{K}_\mathrm{d}$, the unknown induced electric charges. To close the linear system of equations, a set of *non-local Faraday's laws* have to be added, one for each additional unknown. The non-local Faraday's laws can be written on each link $\mathbf{\Lambda}_i$ [§§] as

$$\mathbf{\Pi}^{iT} \mathbf{U} = U_\mathrm{c}^i.$$

[§§] For the sake of parsimony in the notation, since the arrays representing the 1-chain $\mathbf{\Lambda}_i$ and the 1-cochain $\mathbf{\Pi}^i$ are the same, only the former is used in the following.

DOI: 10.1002/nme

By using (36) and (35), they can be written in terms of unknown DoFs as

$$(\mathbf{\Pi}^{iT}\boldsymbol{\eta}\mathbf{C})\mathbf{P}+\sum_{j=1}^{N}(\mathbf{\Pi}^{iT}\boldsymbol{\eta}\mathbf{\Pi}^{j})Q_{\mathrm{c}}^{j}=U_{\mathrm{c}}^{i}-\mathbf{\Pi}^{iT}\boldsymbol{\eta}\mathbf{S}-\sum_{k=N+1}^{N_{\mathrm{c}}}(\mathbf{\Pi}^{iT}\boldsymbol{\eta}\mathbf{\Pi}^{k})Q_{\mathrm{c}}^{k}. \tag{44}$$

It is easy to show that the **P** DoFs involved in each of (44) are that belonging to a pillar of cells pierced by the corresponding link, see Figure 12. As a consequence, the more compact the support of the link is, the fewer fill-in of the system matrix is obtained.

The final algebraic linear system is singular and the so-called *gauge condition* should be applied, for example, by using the standard tree-cotree approach [54]. Nonetheless, using an *ungauged* solution—i.e. without applying a gauge condition—yields a much better result in terms of convergence speed when a preconditioned conjugate gradient solver is used, see [54].

4.5. Computation of the array **S**

A *Spanning Tree Technique* [73, 74] (STT) can be tailored to compute the array **S**, which represents the source charges $\mathbf{Q}_{\mathrm{s}}$. The algorithm is presented in Table I.

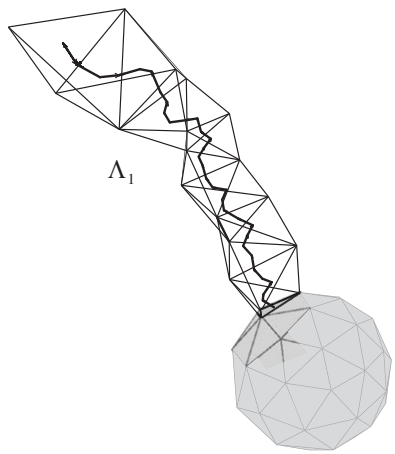

Figure 12. Pillar of cells pierced by the link $\mathbf{\Lambda}_1$.

Table I. The STT algorithm tailored for the computation of the array **S** representing the source charges.

1. $L :=$ all cells $v \in \mathscr{K}_{\mathrm{d}}$ in the dielectric region;
2. `for` every $f \in \mathscr{K}_{\mathrm{d}}$, set $\langle \mathbf{S}, f \rangle :=$ `UNDEFINED`;
3. Find a *facet spanning tree*[a] $\mathfrak{B}$ of $\mathscr{K}_{\mathrm{d}}$;
4. Set $\langle \mathbf{S}, f \rangle := 0$ for all faces $f \in \mathfrak{B}$;
5. `while(` $L \neq \emptyset$)
   (a) `Lsize` $:= card(L)$;
   (b) `for` every $v \in L$
      i. `if` for every $f \in |\partial v|$, $\langle \mathbf{S}, f \rangle \neq$ `UNDEFINED`, `then`
         A. `if` $\langle \mathbf{S}, \partial v \rangle = \langle \mathbf{Q}_{\mathrm{s}}, v \rangle$ `then` $L := L/v$;
         B. `else return FAILURE`;
      ii. `if` there exists a unique $f \in |\partial v|$ such that $\langle \mathbf{S}, f \rangle =$ `UNDEFINED` `then`
         A. Set $\langle \mathbf{S}, f \rangle$ to get $\langle \mathbf{S}, \partial v \rangle = \langle \mathbf{Q}_{\mathrm{s}}, v \rangle$;
         B. $L := L/v$;
   (c) `if` `Lsize` $= card(L)$ `then return INFINITE_LOOP`;
6. `return` **S**;

[a] A facet spanning tree is a tree constructed by using as graph that is obtained by the dual edge–dual node incidence matrix $\langle \mathbf{D}^{\mathrm{T}}, e_{\mathscr{B}} \rangle, \forall e_{\mathscr{B}} \in \mathscr{B}_{\mathrm{d}}$.

DOI: 10.1002/nme

Table II. The GSTT algorithm for the thick links computation.

1. Let $L :=$ all cells $v \in \mathscr{K}_{\mathrm{d}}$ in the dielectric region;
2. `for` every face $f \in \mathscr{K}_{\mathrm{d}}$, set $\langle \mathbf{\Pi}^i, f \rangle :=$ `UNDEFINED`;
3. Find a *facet spanning tree*[a] $\mathfrak{B}$ of $\mathscr{K}_{\mathrm{d}}$, where the faces $f \in \bigcup_{i=1}^{N_{\mathrm{c}}} \Sigma_i$ are set as tree faces at the beginning of the formation of the tree;
4. Select one face $F_i \in \Sigma_i$. Set $\langle \mathbf{\Pi}^i, F_i \rangle := 1$ and $\langle \mathbf{\Pi}^i, f \rangle := 0$ for all $f \in \mathfrak{B}/F_i$;
5. `while(` $L \neq \emptyset$ `)`
   (a) `Lsize` $:= card(L)$;
   (b) `for` every $v \in L$
      ii. `if` for every $f \in |\partial v|$, $\langle \mathbf{\Pi}^i, f \rangle \neq$ `UNDEFINED`, `then`
         A. `if` $\langle \mathbf{\Pi}^i, \partial v \rangle = 0$ `then` $L := L/v$;
         B. `else return FAILURE`;
      ii. `if` there exists a unique $f \in |\partial v|$ such that $\langle \mathbf{\Pi}^i, f \rangle =$ `UNDEFINED` `then`
         A. Set $\langle \mathbf{\Pi}^i, f \rangle$ to get $\langle \mathbf{\Pi}^i, \partial v \rangle = 0$;
         B. $L := L/v$;
   (c) `if Lsize` $= card(L)$ `then return INFINITE_LOOP`;
6. `return` $\mathbf{\Pi}^i$;

[a] A facet spanning tree is a tree constructed by using as graph that is obtained by the dual edge–dual node incidence matrix $\langle \mathbf{D}^{\mathrm{T}}, e_{\mathscr{B}} \rangle, \forall e_{\mathscr{B}} \in \mathscr{B}_{\mathrm{d}}$.

4.6. Automatic computation of links

While cohomology has been fundamental to derive the new geometric formulation based on a vector potential, the use of a cohomology computation to generate the links should be avoided, since it is extremely time consuming. Instead, a couple of more efficient techniques are presented in the following.

4.6.1. Algorithm based on the Generalized Spanning Tree Technique. The *Generalized Spanning Tree Technique* (GSTT) [56, 73, 74] can be tailored to generate the thick links. The GSTT algorithm, described in Table II, works for each conductive region separately. Let us consider the ith conductor $\mathscr{C}_i$. By $card(L)$ we denote the cardinality of the set L.

The proposed algorithm is straightforward to implement and it is very efficient, being the running time linear with the sum of the number of cells and faces in $\mathscr{K}$. It also guarantees, once the algorithm terminates correctly, to return a valid set of coefficients for the thick links [74]. The termination of the GSTT algorithm cannot be proved, since some counter examples have recently been discovered [74]. Nonetheless, if *minimal diameter trees* are used, which are easily constructed by using the *Breadth-first strategy* (BFS) [75], the probability of termination problems is negligible in practice.

We note that the support of the thick links obtained by this algorithm may be in general far from minimal. This is not a serious drawback in practice, but the next algorithm allows the most compact family of thick links to be obtained at a reasonable computational price.

4.6.2. Algorithm based on the shortest path. The most compact family of links can be obtained by means of the shortest paths[¶¶] made of dual edges in $\mathscr{B}_{\mathrm{d}}$ between all possible pairs of dual nodes belonging to each Σ_i and Σ_0, respectively. To find the shortest path between two nodes in a graph, the well-known Dijkstra algorithm may be used, see for example [75, p. 595]. To find the shortest path between all pairs of dual nodes belonging to Σ_i and Σ_0, respectively, a trick can be introduced. Two additional nodes N_0 and N_i are added to the graph. The dual nodes belonging to Σ_0 are connected to N_0, while the dual nodes belonging to Σ_i are connected to N_i. Finally, the shortest path between N_i and N_0 is found with a worst case complexity of $O(e_{\mathrm{g}} + n_{\mathrm{g}} log(n_{\mathrm{g}}))$, where e_{g} is the number of edges in the graph and n_{g} is the number of nodes in the graph. Each

[¶¶] Shortest in the sense of number of dual edges, not in the Euclidean norm sense. The weights of the graphs are set to 1.

DOI: 10.1002/nme

coefficient of the link is recovered as the incidence of the dual edge orientation with respect to the orientation of the path.

5. TAKING ADVANTAGE OF SYMMETRIES

When the electrostatic problem presents some symmetries, the computational domain can be reduced by using the Neumann boundary conditions. In this case, different boundary conditions are imposed on different portions of the external boundary Σ_0, and a generalization is required. Let us present this generalization by means of an example.

Let us consider a parallel plate capacitor with a conducting sphere placed between the plates. The computational domain is bounded by means of symmetry boundary conditions to a box, see on the left of Figure 13. Let us call by S_2 the portion of the external surface Σ_0 subject to symmetry boundary condition and by S_1 the complement of S_2 with respect to $\partial\mathscr{K}_{\mathrm{d}}$. In the example, S_1 is formed by the two non-connected surfaces belonging to Σ_0, corresponding to the plates of the capacitor, plus the boundary of the sphere (hence, S_1 is composed of three distinct connected components), see on the left of Figure 13. One connected component of S_1, called Σ_0', is considered as the new reference conductor in place of the whole Σ_0 and the other N_{c}' connected components of S_1 are considered as boundaries of conductors $\{\mathscr{C}_i\}_{i=1}^{N_{\mathrm{c}}'}$.

5.1. $\mathbf{V}$ *formulation*

The Neumann boundary condition on S_2 is simply obtained by assuming the electric scalar potential $\mathbf{V}$ unknown on the nodes lying on S_2. In fact, Gauss's law (8) is enforced also on a dual cell $v_{\mathscr{B}}$, see Figure 14(a), one-to-one with the node n lying on the considered surface S_2. As one can see in

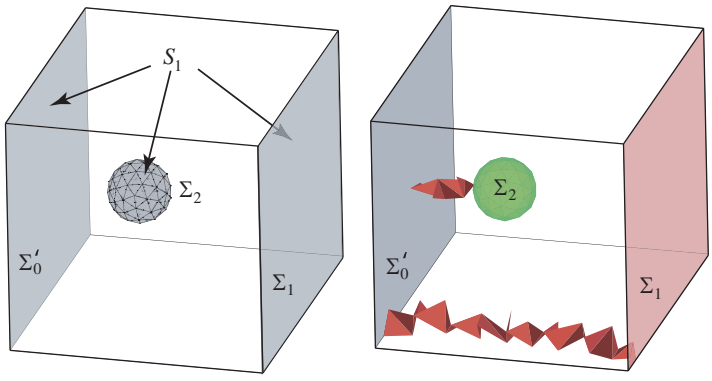

Figure 13. A parallel plate capacitor with a conducting sphere placed between the plates.

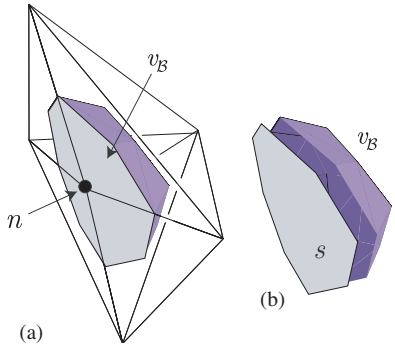

Figure 14. (a) The dual cell $v_{\mathscr{B}}$ lying on the symmetry surface S.
(b) The boundary of $v_{\mathscr{B}}$ contains also the surface s.

DOI: 10.1002/nme

Figure 14(b), the boundary of $v_{\mathscr{B}}$ also contains the surface s, which lies on S_2. Not considering the contribution of the electric flux through the surface s in Gauss's balance law, implicitly enforces this flux to zero. Thus, the electric field E will be tangent to surface S_2.

5.2. **P** *formulation*

Dealing with symmetries, the thick links can be defined as representatives of second cohomology group $H^2(\mathscr{K}_{\mathrm{d}} - S_2)$ generators. By exploiting a well-known duality [57, p. 110], [55]

$$H^2(\mathscr{K}_{\mathrm{d}} - S_2) \cong H_1(\mathscr{B}_{\mathrm{d}}, S_1), \tag{45}$$

the links are defined as representatives of the first relative homology group $H_1(\mathscr{B}_{\mathrm{d}}, S_1)$ generators. Hence, once a connected component of S_1 has been defined as Σ'_0, the links can be obtained as the set of paths formed by dual edges joining Σ'_0 with each other connected component of S_1. In the considered example, the first link joins the two plates of the capacitor, whereas the second joins one plate of the capacitor—which was selected as a reference conductor Σ'_0—to the conducting sphere, see on the right of Figure 13.

The Neumann boundary condition is simply obtained by imposing the vector potential $\langle \mathbf{P}, e \rangle$ to be zero on each edge e belonging to S_2. Hence, the electric field E will be tangent to surface S_2.

Although it is not possible to demonstrate that in general *torsion* [55, 57] vanishes for $H_1(\mathscr{B}_{\mathrm{d}}, S_1)$ (see a counter example in [76]), we conjecture that this is not an issue in practical meaningful problems.

6. NUMERICAL RESULTS

The pair of complementary geometric formulations for electrostatics has been implemented in the CELEKTRO research code [77]. A number of benchmarks solved with the CELEKTRO code are now presented. In the following, by X_r we denote the reference value of the considered physical quantity X, whereas by X_V and X_P we denote the value obtained by the **V** and the **P** formulations, respectively. By X_m we denote the value obtained by computing the mean value $X_m = 0.5(X_V + X_P)$.

6.1. *Benchmark 1*: *spherical capacitor*

The spherical capacitor is composed of two concentric conductive spherical electrodes, see on the left of Figure 15. The radius of the smaller sphere is $a = 20\,\mathrm{m}$, whereas the radius of the bigger sphere

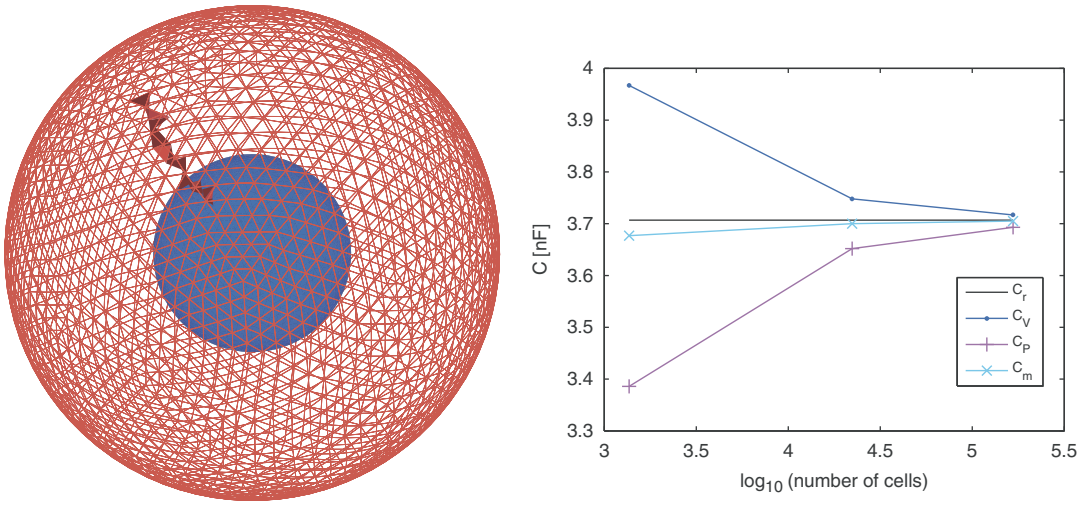

Figure 15. Benchmark problem 1. On the left, the boundary of $\mathscr{K}_{\mathrm{d}}$ and the thick link. On the right, convergence with mesh refinement of the value of capacitance.

DOI: 10.1002/nme

Table III. Convergence with mesh refinement of the capacitance value for Benchmark 1.

# cells in $\mathscr{K}_d$ (meshing time [s])	1365 (1)	22 253 (14)	166 725 (77)
# DoFs **V** (solver time [s])	131 ($\ll 1$)	3204 ($\ll 1$)	25 706 (0.3)
# DoFs **P** (solver time [s])	1909 ($\ll 1$)	27 668 (0.5)	201 266 (8)
C_V [nF] (error %)	3.967 (7.02)	3.748 (1.11)	3.717 (0.28)
C_P [nF] (error %)	3.386 (−8.67)	3.652 (−1.49)	3.693 (−0.37)
C_m [nF] (error %)	3.677 (−0.83)	3.700 (−0.19)	3.705 (−0.047)

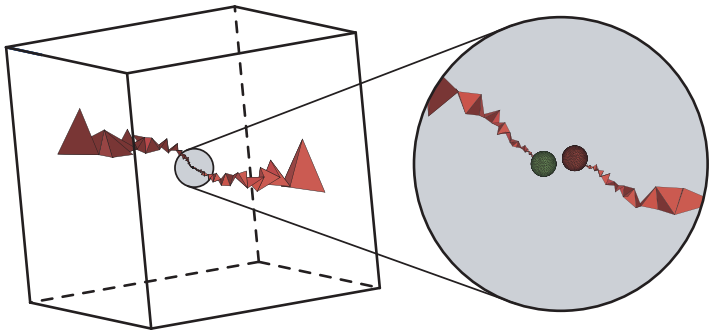

Figure 16. Benchmark problem 2. On the left, the boundary of $\mathscr{K}_d$ and the thick links. On the right, a zoom on the neighborhood of the two spheres.

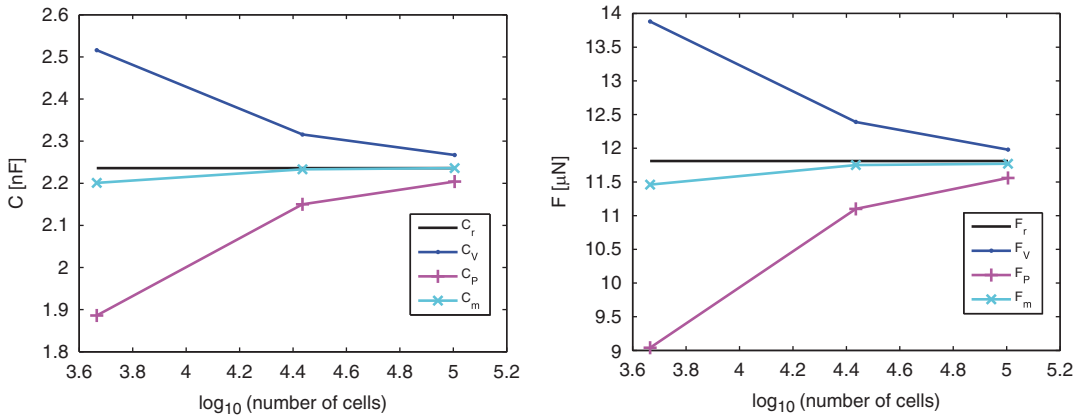

Figure 17. Benchmark problem 2. On the left, convergence with mesh refinement of the value of capacitance between the two spheres. On the right, convergence with mesh refinement of the force between the two spheres.

is $b=50$ m. The reference value is obtained by the formula $C_r=4\pi\varepsilon_0/(1/a+1/b)=3.7071$ nF. On the right of Figure 15 and in Table III, the results in terms of the convergence of the capacitance value with mesh refinement are shown.

6.2. *Benchmark 2*: *two conducting spheres*

A benchmark composed of two equal conductive spheres is proposed, see Figure 16. The radius of the spheres is $r=25$ m and the distance between the two centers is $d=70$ m. The potential $V_1=-50$ V is assigned to the first sphere and the potential $V_2=50$ V is assigned to the second sphere. The two spheres are placed inside an external cube having an edge length of 10 km. The value of the capacitance is calculated analytically by means of the method of image charges [78, 79] $C=2.2364\times10^{-9}$ F. The attractive force acting on the direction identified by the line which connects the two centers of the spheres is analytically computed by evaluating $F=(U^2/2)\partial C/\partial x=1.1812\times10^{-7}$ N. In Figure 17 and in Table IV the results in terms of the convergence of the values

DOI: 10.1002/nme

Table IV. Convergence with mesh refinement of the capacitance value and force for Benchmark 2.

# cells in $\mathscr{K}_d$ (meshing time [s])	4626 (2.3)	27 259 (15.9)	101 183 (53.2)
# DoFs **V** (solver time [s])	716 ($\ll 1$)	4307 ($\ll 1$)	16 373 (0.3)
# DoFs **P** (solver time [s])	5665 ($\ll 1$)	32 979 (1)	121 311 (10.5)
C_V [nF](error %)	2.516 (12.5)	2.316 (3.57)	2.267 (1.38)
C_P [nF](error %)	1.886 (−15.67)	2.150 (−3.84)	2.204 (−1.44)
C_m [nF](error %)	2.201 (−1.57)	2.233 (−0.27)	2.236 (−0.032)
F_V [μN](error %)	13.88 (17.48)	12.39 (4.91)	11.98 (1.47)
F_P [μN](error %)	9.040 (−23.45)	11.10 (−6.01)	11.56 (−2.08)
F_m [μN](error %)	11.46 (−2.98)	11.75 (−0.55)	11.77 (−0.31)

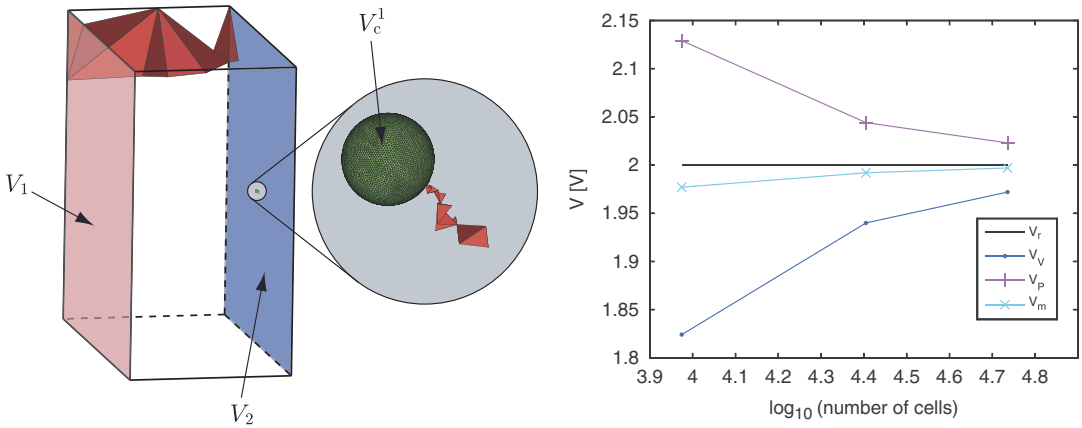

Figure 18. Benchmark problem 3. On the left, the boundary of $\mathscr{K}_d$ and the thick links. On the right, convergence with mesh refinement of the sphere's potential value.

of capacitance and force with mesh refinement are shown. The force is computed by using the technique described in [80].

6.3. *Benchmark 3*: *conducting sphere with floating potential constraint in a uniform electric field*

A conducting sphere is placed between two parallel electrodes, see on the left of Figure 18. Let us assume that the distance of the two electrodes is $d=10.5$ m and the radius of the sphere is $R=0.1$ m. The sphere is placed at a distance of $h=0.25$ m from the second electrode. Over the electrodes 1 and 2 the potentials $V_1=-1$ V and $V_2=0$ V, respectively, are applied by the Dirichlet boundary conditions. Let us fix the potential on the boundary of the conducting sphere, again with the Dirichlet boundary conditions, at $V_c^1=2$ V. The closed-form expression for the total charge Q_{tot}^1 on the sphere, described in [81], is

$$Q_{\text{tot}}^1=4\pi\varepsilon R^2\left(k_1\sum_{n=1}^{\infty}\frac{1}{\sinh(na)}+k_2\sum_{n=1}^{\infty}\frac{\cosh(na)}{\sinh^2(na)}\right) \tag{46}$$

where $\cosh(a)=h/R$, $k_1=(V_c^1/h)\sinh(a)\cosh(a)$, $k_2=(V_0/d)\sinh^2(a)$. Evaluating Q_{tot}^1 for the proposed benchmark yields $Q_{\text{tot}}^1=28.188$ pC.

The computational domain is truncated by considering an extension of the electrodes equal to $L=10$ m and meshed with an unstructured tetrahedral mesh. In this benchmark, to test the floating potential constraint, a total charge of $Q_{\text{tot}}^1=28.188$ pC is assigned on the surface of the sphere (instead of assigning the potential $V_c^1=2$ V). The potentials $V_1=-1\,V$ and $V_2=0\,V$, respectively, are enforced by the Dirichlet boundary conditions on the electrodes 1 and 2, while a Neumann boundary condition is imposed on the other external surfaces. The values of V_c^1 computed by using meshes with increasing refinement are visible in Table V and on the right of Figure 18.

DOI: 10.1002/nme

Table V. Convergence with mesh refinement of the sphere's potential for Benchmark 3.

# cells in $\mathscr{K}_{\mathrm{d}}$ (meshing time [s])	9424 (4.1)	25 415 (15.6)	54 408 (30.2)
# DoFs **V** (solver time [s])	1213 ($\ll 1$)	3550 ($\ll 1$)	8425 ($\ll 1$)
# DoFs **P** (solver time [s])	12 111 (0.2)	31 969 (0.7)	66 167 (1.9)
V_V[nF](error %)	1.824 (−8.77)	1.940 (−2.98)	1.972 (−1.42)
V_P[nF](error %)	2.129 (6.43)	2.044 (2.18)	2.023(1.19)
V_m[nF](error %)	1.977 (−1.17)	1.992 (−0.40)	1.997 (−0.12)

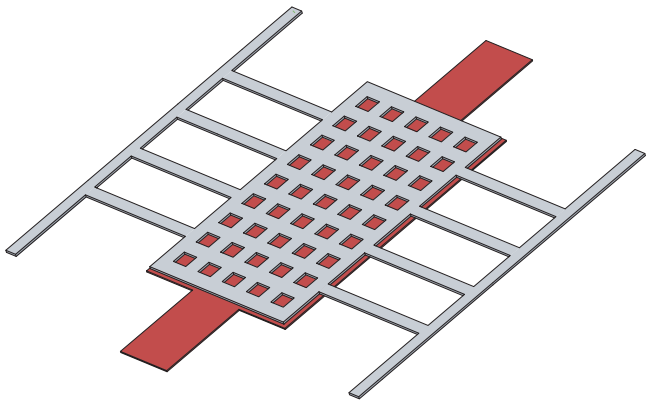

Figure 19. Benchmark problem 4: The geometry of the considered electrostatic MEMS.

6.4. *Benchmark 4*: *capacitance of an MEMS switch*

As an industrial test case, the capacitive MEMS switch benchmark described in [82] is used, see Figure 19. The MEMS is composed of a perforated top plate (475 μm height, 275 μm width, thickness 4 μm) suspended by a set of beams over a bottom plate (485 μm height, 285 μm width, thickness 0.5 μm, gap 3 μm). The bottom plate is coated with a thin dielectric layer ($\varepsilon_r = 7$) of thickness 0.2 μm. The dimension of the holes in the top plate is 25×25 μm with a pitch of 50 μm. The MEMS is placed in the center of a cube with edge length of 20 mm. The other geometric parameters can be obtained from Figure 20.

The MEMS capacitance is computed in [82] by using three softwares:

- Femlab (http://www.comsol.com) $C_{\mathrm{F}} = 0.37$ pF;
- COVENTOR (http://www.coventor.com) $C_{\mathrm{C}} = 0.40$ pF;
- GetDp (http://www.geuz.org/getdp/) $C_{\mathrm{G}} = 0.36$ pF.

The results obtained by using the CELEKTRO code are reported in Table VI.

7. CONCLUSIONS

A pair of complementary geometric formulations for electrostatics suitable with polyhedral meshes has been introduced. The design of the potentials employed in the vector potential-based formulation has been formally presented by using the tools from homology and cohomology theories with integer coefficients. It has been shown how a family of thick links is needed, which are the representatives of generators for the second cohomology group over integers of the dielectric region. Two automatic and efficient graph-theoretic algorithms to find the thick links have been introduced. In particular, the second algorithm produces the most compact family of thick links, minimizing the fill-in of the system of equations sparse matrix. The original non-local equations arising in both formulations when imposing boundary conditions have been described in detail.

As the numerical results confirm, the values obtained by the two formulations provide the upper and lower bounds for each electromagnetic quantity and their average results quite close to the

DOI: 10.1002/nme

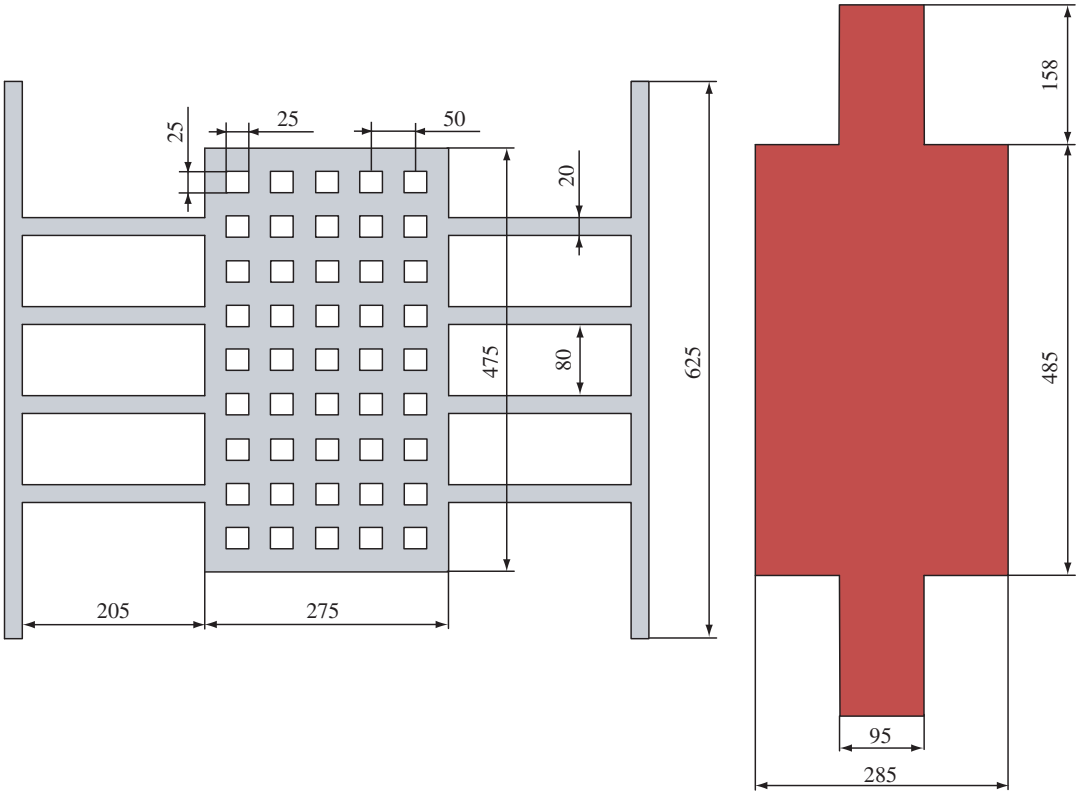

Figure 20. Geometry of benchmark problem 4. (All dimensions are in μm.)

Table VI. Convergence with mesh refinement of the capacitance value for Benchmark 4.

# cells in $\mathscr{K}_{\mathrm{d}}$ (meshing time [s])	30 456 (36.4)	252 096 (190.0)	573 952 (373.5)
# DoFs **V** (solver time [s])	3136 ($\ll 1$)	34 236 (0.4)	64 876 (0.5)
# DoFs **P** (solver time [s])	40 440 (2.4)	316 172 (29.2)	766 396 (77.1)
C_V [nF]	0.408	0.390	0.385
C_P [nF]	0.316	0.345	0.355
C_m [nF]	0.362	0.368	0.370

exact solution even for extremely coarse meshes. To conclude, complementarity should be always exploited, since it allows saving at least an order of magnitude of mesh elements maintaining the same accuracy. This has a big impact on the computational time, since the mesh generation is the most computationally expensive task.

ACKNOWLEDGEMENTS

The author thank Paweł Dłotko (Institute of Computer Science, Jagiellonian University, Kraków, Poland) for many useful discussions and suggestions.

REFERENCES

1. Kao WH, Lo C-Y, Basel M, Singh R. Parasitic extraction: current state of the art and future trends. *Proceedings of the IEEE* 2001; **89**(5):729–739.
2. Yu W, Wang Z. Capacitance extraction. In *Encyclopedia of RF and Microwave Engineering*, Chang K (ed.). Wiley: New York, 2005.
3. Kim Y, Petranovic D, Sylvester D. Simple and accurate models for capacitance considering floating metal fill insertion. *IEEE Transactions on VLSI Systems* 2009; **17**(8):1166–1170.

DOI: 10.1002/nme

4. Yu W, Zhang M, Wang Z. Efficient 3-D extraction of interconnect capacitance considering floating metal-fills with boundary element method. *IEEE Transactions on Computer-Aided Design* 2006; **25**(1):12–18.
5. Ansoft® Q3D EXTRACTOR™. Available from: http://www.ansoft.com.
6. Cadence® QRC EXTRACTION™. Available from: http://www.cadence.com.
7. Mentor Graphics® CALIBRE xRC™. Available from: http://www.mentor.com.
8. Magma® QUICKCAP™. Available from: http://www.magma-da.com.
9. Simucad® HIPEX™. Available from: http://www.simucad.com.
10. Synopsys® RAPHAEL NXT™. Available from: http://www.synopsys.com.
11. OptEM Engineering® OPTEM INSPECTOR™. Available from: http://www.optem.com.
12. CST® EM STUDIO™. Available from: http://www.cst.com.
13. Stine BE, Boning DS, Chung JE, Camilletti L, Kruppa F, Equi ER, Loh W, Prasad S, Muthukrishnan M, Towery D, Berman M, Kapoor A. The physical and electrical effects of metal-fill patterning practices for oxide chemical-mechanical polishing processes. *IEEE Transactions on Electron Devices* 1998; **45**(3):665–679.
14. Kahng AB, Samadi K. CMP fill synthesis: a survey of recent studies. *IEEE Transactions on CAD of Integrated Circuits and Systems* 2008; **27**(1):3–19.
15. Anderson CR. Efficient solution of the Schroedinger–Poisson equations in layered semiconductor devices. *Journal of Computational Physics* 2009; **228**:4745–4756.
16. Trellakis A, Galick AT, Pacelli A, Ravaioli U. Iteration scheme for the solution of the two-dimensional Schrödinger–Poisson equations in quantum structures. *Journal of Applied Physics* 1997; **81**:7880–7884.
17. Abdel-Rahman EM, Younis MI, Nayfeh AH. Characterization of the mechanical behavior of an electrically actuated microbeam. *Journal of Micromechanics and Microengineering* 2002; **12**(6):759–766.
18. Bettini P, Brusa E, Munteanu M, Specogna R, Trevisan F. Innovative numerical methods for nonlinear MEMS: the non-incremental FEM vs the discrete geometric approach. *Computer Modeling in Engineering and Sciences* 2008; **33**(3):215–242.
19. Bettini P, Brusa E, Munteanu M, Specogna R, Trevisan F. Static behaviour prediction of microelectrostatic actuators by discrete geometric approaches. *IEEE Transactions on Magnetics* 2008; **44**(6):1606–1609.
20. De Lorenzi A, Grando L, Gobbo R, Pesavento G, Bettini P, Specogna R, Trevisan F. The insulation structure of the 1 MV transmission line for the ITER neutral beam injector. *Fusion Engineering and Design* 2007; **82**(5–14):836–844.
21. De Lorenzi A, Grando L, Pesce A, Bettini P, Specogna R. Modeling of epoxy resin spacers for the 1 MV dc gas insulated line of ITER neutral beam injector system. *IEEE Transactions on Dielectrics and Electrical Insulation* 2009; **16**(1):77–87.
22. Kron G. Numerical solution of ordinary and partial differential equations by means of equivalent circuits. *Journal of Applied Physics* 1945; **126**:172–186.
23. Branin FH. The algebraic-topological basis for network analogies and the vector calculus. *Proceedings of the Symposium on Generalized Network*. Polytechnic Press: Brooklin, NY, 1966; 453–491.
24. Tonti E. On the formal structure of physical theories. Monograph of the Italian National Research Council, 1975 (available online).
25. Weiland T. A discretization method for the solution of Maxwell's equations for six-component fields. *Electronic Communications* (*AEÜ*) 1977; **31**(3):116.
26. Deschamps GA. Electromagnetics and differential forms. *Proceedings of the IEEE* 1981; **69**(6):676–696.
27. Tonti E. On the geometrical structure of the electromagnetism. In *Gravitation*, *Electromagnetism and Geometrical Structures*, for the 80th Birthday of Lichnerowicz A, Ferrarese G (ed.). Pitagora Editrice: Bologna, 1995; 281–308.
28. Mattiussi C. An analysis of finite volume, finite element and finite difference methods using some concepts from algebraic topology. *Journal of Computational Physics* 1997; **133**:289–309.
29. Bossavit A. How weak is the Weak Solution in finite elements methods? *IEEE Transactions on Magnetics* 1998; **34**(5):2429–2432.
30. Tonti E. Algebraic topology and computational electromagnetism. *Fourth International Workshop on Electric and Magnetic Fields*, Marseille (Fr), 12–15 May 1998; 284–294.
31. Tarhasaari T, Kettunen L, Bossavit A. Some realizations of a discrete Hodge operator: a reinterpretation of finite element techniques. *IEEE Transactions on Magnetics* 1999; **35**:1494–1497.
32. Teixeira FL, Chew WC. Lattice electromagnetic theory from a topological viewpoint. *Journal of Mathematical Physics* 1999; **40**(1):169–187.
33. Bossavit A, Kettunen L. Yee-like schemes on staggered cellular grids: a synthesis between FIT and FEM approaches. *IEEE Transactions on Magnetics* 2000; **36**(4):861–867.
34. Tonti E. Finite formulation of the electromagnetic field. *Progress in Electromagnetics Research* (*PIER 32*) (*Special Volume on Geometrical Methods for Computational Electromagnetics*). EMW: Boston, 2001; 1–44. Available from: http://www.jpier.org/PIER/.
35. Chew WC. Electromagnetic theory on a lattice. *Journal of Applied Physics* 2001; **75**(10):4843–4850.
36. Tonti E. Finite formulation of the electromagnetic field. *IEEE Transactions on Magnetics* 2002; **38**(2):333–336.
37. Hirani AN. Discrete exterior calculus. *Ph.D. Dissertation*, California Institute of Technology, 2003.
38. Hyman JM, Shashkov M. Mimetic discretizations for Maxwell's equations. *Journal of Computational Physics* 1999; **151**(2):881–909.

DOI: 10.1002/nme

39. Bochev PV, Hyman JM. Principles of mimetic discretizations of differential operators. In *Proceedings of IMA Hot Topics workshop on Compatible Spatial Discretizations*, *IMA 142*, Arnold D, Bochev P, Lehoucq R, Nicolaides R, Shashkov M (eds). Springer: Berlin, 2006; 89–119.
40. Brezzi F, Lipnikov K, Shashkov M. Convergence of the mimetic finite difference method for diffusion problems on polyhedral meshes. *SIAM Journal on Numerical Analysis* 2005; **43**:1872–1896.
41. Brezzi F, Buffa A, Lipnikov K. Mimetic finite differences for elliptic problems. *ESAIM*: *Mathematical Modelling and Numerical Analysis* 2009; **43**:277–295.
42. Brezzi F, Fortin M. *Mixed and Hybrid Finite Element Methods*. Springer: New York, 1991.
43. Brezzi F, Douglas J, Marini D. Two families of mixed finite elements for 2nd order elliptic problems. *Numerische Mathematik* 1985; **47**:217–235.
44. Cosmi F. Numerical solution of plane elasticity problems with the cell method. *Computer Modeling in Engineering and Sciences* 2001; **2**:365–372.
45. Yavari A. On geometric discretization of elasticity. *Journal of Mathematical Physics* 2008; **49**:022901.
46. Tonti E, Zarantonello F. Algebraic formulation of elastostatics: the cell method. *Computer Modeling in Engineering and Sciences* 2009; **39**(3):201–236.
47. Tonti E, Zarantonello F. Algebraic formulation of elastodynamics: the cell method. *Computer Modeling in Engineering and Sciences* 2010; **64**(1):37–70.
48. Arthurs AM. *Complementary Variational Principles*. Oxford University Press: Oxford, 1970.
49. Oden JT, Reddy JN. On dual-complementary variational principles in mathematical physics. *International Journal of Engineering Science* 1974; **12**:1–29.
50. Penman J, Fraser JR. Dual and complementary energy methods in electromagnetism. *IEEE Transactions on Magnetics* 1983; **19**(6):2311–2316.
51. Penman J, Fraser JR, Smith JR, Grieve MD. Complementary energy methods in the computation of electrostatic fields. *IEEE Transactions on Magnetics* 1983; **19**(6):2288–2291.
52. Rikabi JAH, Bryant CF, Freeman EM. Complementary solutions of electrostatic field problems. *IEEE Transactions on Magnetics* 1989; **25**:4427–4442.
53. Golias NA, Tsiboukis TD, Bossavit A. Constitutive inconsistency: rigorous solution of Maxwell equations based on a dual approach. *IEEE Transactions on Magnetics* 1994; **30**:3586–3589.
54. Ren Z. A 3D vector potential formulation using edge element for electrostatic field computation. *IEEE Transactions on Magnetics* 1995; **31**:1520–1523.
55. Munkres JR. *Elements of Algebraic Topology*. Perseus Books: Cambridge, MA, 1984.
56. Dłotko P, Specogna R, Trevisan F. Automatic generation of cuts on large-sized meshes for the T-Ω geometric eddy-current formulation. *Computer Methods in Applied Mechanics and Engineering* 2009; **198**:3765–3781.
57. Gross PW, Kotiuga PR. *Electromagnetic Theory and Computation*: *A Topological Approach*, vol. 48. Cambridge University Press: Cambridge, MA, U.S.A., 2004; ISBN: 0521801605.
58. Bott R, Tu LW. *Differential Forms in Algebraic Topology*. Springer: Berlin, 1982.
59. Dłotko P, Specogna R. Efficient cohomology computation for electromagnetic modeling. *Computer Modeling in Engineering and Sciences* 2010; **60**:247–278.
60. Nicolet A, Remacle J-F, Meys B, Genon A, Legros W. Transformation methods in computational electromagnetics. *Journal of Applied Physics* 1994; **75**(10):6036–6038.
61. Suuriniemi S, Kangas J, Kettunen L, Tarhasaari T. Detection of state variables for coupled circuit-field problems. *IEEE Transactions on Magnetics* 2004; **40**(2):949–952.
62. Dodziuk J. Finite-difference approach to the Hodge theory of harmonic forms. *Americal Journal of Mathematics* 1976; **98**(1):79–104.
63. Specogna R, Trevisan F. Discrete constitutive equations in A-χ geometric eddy-currents formulation. *IEEE Transactions on Magnetics* 2005; **41**(4):1259–1263.
64. Bossavit A. Computational electromagnetism and geometry. (5): The 'Galerkin hodge'. *Journal of Japan Society of Applied Electromagnetics and Mechanics* 2000; **8**(2):203–209.
65. Codecasa L, Specogna R, Trevisan F. Symmetric positive-definite constitutive matrices for discrete eddy-current problems. *IEEE Transactions on Magnetics* 2007; **42**(2):510–515.
66. Codecasa L, Specogna R, Trevisan F. Base functions and discrete constitutive relations for staggered polyhedral grids. *Computer Methods in Applied Mechanics and Engineering* 2009; **198**(9–12):1117–1123.
67. Codecasa L, Specogna R, Trevisan F. A new set of basis functions for the discrete geometric approach. *Journal of Computational Physics* 2010; **229**:7401–7410.
68. Codecasa L, Specogna R, Trevisan F. Subgridding to solving magnetostatics within discrete geometric approach. *IEEE Transactions on Magnetics* 2009; **45**(3):1024–1027.
69. Dular P, Legros W, Nicolet A. Coupling of local and global quantities in various finite element formulations and its application to electrostatics, magnetostatics and magnetodynamics. *IEEE Transactions on Magnetics* 1998; **34**:3078–3081.
70. De Gersem H, Belmans R, Hameyer K. Floating potential constraints and field-circuit couplings for electrostatic and electrokinetic finite element models. *COMPEL* 2003; **22**:20–29.
71. Kettunen L, Forsman K, Bossavit A. Discrete spaces for div and curl-free fields. *IEEE Transactions on Magnetics* 1998; **34**:2551–2554.
72. Massey WS. *Singular Homology Theory*. Springer: New York, 1980.

DOI: 10.1002/nme

73. Bossavit A. *Computational Electromagnetism*. Academic Press: San Diego, U.S.A., 1998. Available from: http://butler.cc.tut.fi/bossavit/.
74. Dłotko P, Specogna R. Critical analysis of the spanning tree techniques. *SIAM Journal on Numerical Analysis* 2010; **48**:1601–1624.
75. Cormen TH, Leiserson CE, Rivest RL, Stein C. *Introduction to Algorithms* (2nd edn). MIT Press: Cambridge, MA, U.S.A., 2001.
76. Suuriniemi S. Homological computations in electromagnetic modeling. *Ph.D. Thesis*, Tampere University of Technology, Tampere, Finland, 2004; ISBN: 952-15-1237-7.
77. Specogna R. CELEKTRO: complementary electrostatic and electro-quasistatic solvers, copyright 2008–2010. Available from: http://www.celektro.com.
78. Durand E. *Électrostatique*, *Tome II*: *Problèmes Généraux*, *Conducteurs*. Masson: Paris, 1966; ISBN: 2225520968.
79. Liu J, Shirkoohi GH, Freeman EM. The calculation of capacitance and force in electrostatic fields by using the boundary element method. *IEEE Transactions on Magnetics* 1992; **28**:1072–1075.
80. Henrotte F, Specogna R, Trevisan F. Reinterpretation of the Nodal Force Method within discrete geometric approaches. *IEEE Transactions on Magnetics* 2008; **44**(6):690–693.
81. Pérez AT. Charge and force on a conducting sphere between two parallel electrodes. *Journal of Electrostatics* 2002; **56**:199–217.
82. Sabariego RV, Gyselinck J, Dular P, De Coster J, Henrotte F, Hameyer K. Coupled mechanical-electrostatic FE-BE analysis with FMM acceleration: application to a shunt capacitive MEMS switch. *COMPEL* 2004; **23**:876–884.

DOI: 10.1002/nme